Eur. Phys. J. C (2018) 78:155
https://doi.org/10.1140/epjc/s10052-018-5625-3

THE EUROPEAN PHYSICAL JOURNAL C

Special Article - Tools for Experiment and Theory

CP-violating top quark couplings at future linear e^+e^- colliders

W. Bernreuther[1], L. Chen[1,4], I. García[2,5,a], M. Perelló[2], R. Poeschl[3], F. Richard[3], E. Ros[2], M. Vos[2]

[1] Institut für Theoretische Teilchenphysik und Kosmologie, RWTH Aachen University, 52056 Aachen, Germany
[2] Instituto de Física Corpuscular (IFIC, UVEG/CSIC), Apartado de Correos 22085, 46071 Valencia, Spain
[3] Laboratoire de l'Accélérateur Linéaire (LAL), Centre Scientifique d'Orsay, 91898 Orsay Cedex, France
[4] *Present address:* Max-Planck-Institut f. Physik, 80805 Munich, Germany
[5] *Present address:* CERN, 1211, Geneva 23, Switzerland

Received: 24 October 2017 / Accepted: 9 February 2018 / Published online: 23 February 2018

Abstract We study the potential of future lepton colliders to probe violation of the CP symmetry in the top quark sector. In certain extensions of the Standard Model, such as the two-Higgs-doublet model (2HDM), sizeable anomalous top quark dipole moments can arise, which may be revealed by a precise measurement of top quark pair production. We present results from detailed Monte Carlo studies for the ILC at 500 GeV and CLIC at 380 GeV and use parton-level simulations to explore the potential of high-energy operation. We find that precise measurements in $e^+e^- \to t\bar{t}$ production with subsequent decay to lepton plus jets final states can provide sufficient sensitivity to detect Higgs-boson-induced CP violation in a viable two-Higgs-doublet model. The potential of a linear e^+e^- collider to detect CP-violating electric and weak dipole form factors of the top quark exceeds the prospects of the HL-LHC by over an order of magnitude.

1 Introduction

The top quark is by far the heaviest fundamental particle known to date. Its large mass implies that it is the Standard Model particle that is most strongly coupled to the electroweak symmetry breaking sector. The top quark is also set apart from the other quarks in that it does not form hadronic bound-states – that is, it offers the possibility to study the interactions of a bare quark. The experimental investigation of single-top and top-quark pair production at the Tevatron and at the large hadron collider (LHC) has led to a precise knowledge of the top-quark strong and weak charged-current interactions. These results are in good agreement with the Standard Model (SM) predictions.

The electroweak neutral current interactions of the top quark are much less precisely investigated. At the LHC an accurate measurement of the top-quark neutral current couplings to the photon (γ) and Z boson is challenging, because $t\bar{t}$ pairs are dominantly produced by the strong interactions, and the associated production of $t\bar{t}$ and a hard photon or Z boson is relatively rare compared to the production of $t\bar{t}$ + jets. Future lepton colliders will offer the opportunity to precisely explore these top-quark interactions. The studies in Refs. [1–7] have shown that linear collider (LC) experiments can measure the top-quark electroweak couplings with very competitive precision.

Several projects exist for e^+e^- colliders with sufficient energy to produce top-quark pairs (i.e., with centre-of-mass energy $\sqrt{s} > 2m_t$). A mature design exists for a linear e^+e^- collider that can ultimately reach centre-of-mass energies up to approximately 1 TeV, the international linear collider (ILC) [8], to be hosted in Japan. We focus on the planned operation at a centre-of-mass energy of 500 GeV, consider the initial integrated luminosity scenario (500 fb^{-1}) and the nominal H20 scenario [9] (4 ab^{-1}).

Extensive R&D into high-gradient acceleration has, moreover, opened up the possibility of a relatively compact multi-TeV collider, the compact linear collider (CLIC) [10]. The CLIC program envisages an initial stage that collects approximately 500 fb^{-1} at $\sqrt{s} = 380$ GeV, followed by operation at a centre-of-mass energy of up to 3 TeV [11].

Both linear collider projects offer the possibility of polarized beams. Operation of the collider with two polarization configurations allows one to disentangle the photon and Z-boson form factors. ILC and CLIC both envisage polarizing the electron beam (80% longitudinal polarization). The ILC baseline design envisages 30% positron polarization. In the CLIC design this is left as an upgrade option.

ILC and CLIC have developed detailed detector designs and sophisticated simulation and reconstruction software, which allows a careful study of experimental effects in realistic conditions. Here, we perform a full simulation of the

[a] e-mail: ignacio.garcia@ific.uv.es

reaction $e^+e^- \to t\bar{t} \to$ lepton plus jets in the context of these projects.

In this paper we extend the studies of Refs. [1,12] to couplings that violate the combination of charge conjugation and parity (CP, in the following). New physics that affects top-quark production and/or decay is parametrized in terms of form factors that depend on kinematic invariants. The Standard Model predicts CP violation in top-quark pair production and decay to be very small, well beyond the experimental sensitivity of existing and planned facilities (see the discussion in Sect. 9). Some extensions of the SM, such as, for instance, two-Higgs-doublet models, can give rise to sizeable effects [13]. Any observation of CP violation in the top-quark sector would be clear evidence of physics beyond the SM. Early studies of non-standard CP violation (i.e. CP violation that is not induced by the Kobayashi–Maskawa CP phase) in $e^+e^- \to t\bar{t}$ include those in Refs. [14–16]. Our study is based on the observables proposed in Ref. [17] for the lepton plus jets final states that have a direct sensitivity to the electric and weak dipole form factors of the top quark. We present the first result of a detailed Monte Carlo simulation of these observables in a realistic experimental environment.

This paper is organized as follows. Section 2 describes our conventions for the form factors with which one can parametrize top-quark pair production at lepton colliders. We analyze in Sect. 3 the potential magnitude of the CP-violating top-quark electric and weak dipole form factors in two SM extensions taking into account present experimental constraints. Moreover, we briefly discuss the potential magnitude of CP-violating form factors in top-quark decay, $t \to Wb$. Observables and associated asymmetries sensitive to CP violation in $t\bar{t}$ production which apply to lepton plus jets final states are introduced in Sect. 4. We study the effect of polarized beams in Sect. 5 and determine the relations between the CP asymmetries and CP-violating form factors. Full-simulation results at two centre-of-mass energies are presented in Sect. 6 for the ILC at 500 GeV and in Sect. 7 for CLIC at 380 GeV. In Sect. 8 we study the prospect of $1-3$ TeV operation in a parton-level study. Systematic uncertainties are discussed in Sect. 9. The prospects of linear e^+e^- colliders for the extraction of the CP-violating form factors derived in this study are presented in Sect. 10 and compared with other studies in the literature of the potential of lepton and hadron colliders. We conclude in Sect. 11.

2 CP violation in $e^+e^- \to t\bar{t}$

Our present knowledge of physics at the TeV scale implies that in e^+e^- collisions at centre-of-mass (c.m.) energies $\lesssim 1$ TeV top-quark pairs will be dominantly produced by SM interactions, to wit, by s-channel photon and Z-boson exchange. New physics interactions that involve the top quark may modify the $t\bar{t}X$ ($X = \gamma, Z$) vertices and the overall $e^+e^- \to t\bar{t}$ production amplitude. In order to pursue a relatively model-independent analysis, we assume that new CP-violating interactions, which can lead to sizeable effects in $t\bar{t}$ production, have only a small effect on top-quark decay. We will discuss in Sect. 3 the validity of this assumption within two SM extensions.

Lorentz covariance determines the structure of the $t\bar{t}X$ vertex. In the case that both top quarks are on their mass shell and the photon and Z-boson are off-shell we can write the $t\bar{t}X$ vertex as

$$\Gamma^{ttX}_{\mu}(k^2) = -ie\Big\{\gamma_\mu\left(F^X_{1V}(k^2) + \gamma_5 F^X_{1A}(k^2)\right) + \frac{\sigma_{\mu\nu}k^\nu}{2m_t}\left(iF^X_{2V}(k^2) + \gamma_5 F^X_{2A}(k^2)\right)\Big\}, \quad (1)$$

where $e = \sqrt{4\pi\alpha}$, with α the electromagnetic fine structure constant, m_t denotes the mass of the top quark, and $k^\mu = q^\mu + \bar{q}^\mu$ is the sum of the four-momenta q^μ and $\bar{q}^\mu$ of the t and $\bar{t}$ quark. We use $\gamma_5 = i\gamma^0\gamma^1\gamma^2\gamma^3$ and $\sigma_{\mu\nu} = \frac{i}{2}\left(\gamma_\mu\gamma_\nu - \gamma_\nu\gamma_\mu\right)$. The F_i denote form factors which are to be probed in the time-like domain $k^2 > 4m_t^2$ by the reaction at hand.[1]

For off-shell γ, Z bosons, there are in general two more contributions, one of which could violate CP invariance. However, if the mass of the electron is neglected, an excellent approximation in our case, these two terms will not contribute to the $t\bar{t}$ production amplitude. We therefore omit them in the following.

Within the Standard Model, and at tree level, the F_1 are related to the electric charge of the top quark Q_t and its weak isospin:

$$F^{\gamma,\mathrm{SM}}_{1V} = Q_t = -\frac{2}{3},\ F^{\gamma,\mathrm{SM}}_{1A} = 0,$$
$$F^{Z,\mathrm{SM}}_{1V} = -\frac{1}{4s_W c_W}\left(1 - \frac{8}{3}s_W^2\right),\ F^{Z,\mathrm{SM}}_{1A} = \frac{1}{4s_W c_W}, \quad (3)$$

where s_W and c_W are the sine and the cosine of the weak mixing angle θ_W. The chirality-flipping form factors F_2 are zero at tree level. As in any renormalisable theory they must be loop-induced. At zero momentum transfer $F^\gamma_{2V}(0)$ is related via $F^\gamma_{2V}(0) = Q_t(g_t - 2)/2$ to the anomalous magnetic moment of the top quark g_t, where Q_t denotes its electrical charge in units of e.

In this paper we focus on the form factors F^X_{2A} that violate the combined charge and parity symmetry CP. The electric dipole moment of the top quark is determined by

[1] The form factors F_i are related to the $\tilde{F}_i$ of Ref. [18] through the following relations:
$\tilde{F}^X_{1V} = -\left(F^X_{1V} + F^X_{2V}\right),\quad \tilde{F}^X_{2V} = F^X_{2V},$
$\tilde{F}^X_{1A} = -F^X_{1A},\quad \tilde{F}^X_{2A} = -iF^X_{2A}.$ (2)

F_{2A}^{γ} for an on-shell photon at zero momentum transfer, $d_t^{\gamma} = -(e/2m_t)F_{2A}^{\gamma}(0)$. In analogy with this relation one may define an electric dipole form factor (EDF) and a weak dipole form factor (WDF) for on-shell $t, \bar{t}$ but off-shell γ, Z:

$$d_t^X(k^2) = -\frac{e}{2m_t}F_{2A}^X(k^2), \quad X = \gamma, Z. \tag{4}$$

For off-shell gauge bosons these form factors are in general gauge-dependent. However, within the two SM extensions that will be discussed in the next section, the $d_t^X(s)$ are gauge-invariant to one-loop approximation. This may justify their use in parametrizing possible CP-violating effects in $t\bar{t}$ production.

Finally, we note that new physics effects are often described in the framework of effective field theory (EFT) by anomalous couplings, i.e., constants. The 'couplings' d_t^{γ} and d_t^Z can be related to the coefficients of certain dimension-six operators; cf., for instance, Ref. [19]. However, by using EFT for describing new physics one assumes that there is a gap between the typical energy scale of the process under consideration ($\sqrt{s}$ in our case) and the scale of new physics. This is not the case for the models that we consider in the next section. In particular, in the kinematic domain that we are interested in, d_t^{γ} and d_t^Z show a non-negligible dependence on $\sqrt{s}$ and can develop absorptive parts, therefore becoming complex.

3 CP-violation in SM extensions

In the SM, where CP violation is induced by the Kobayashi–Maskawa (KM) phase in the charged weak current interactions, resulting CP effects in flavour-diagonal amplitudes are too small to be measurable in $e^+e^- \to t\bar{t}$ [13]. Sizeable CP-violating effects involving top quarks may arise in SM extensions with additional, non-KM CP-violating interactions. In this section we consider two extensions of this type, namely two-Higgs-doublet models and the mimimal supersymmetric extension of the Standard Model (MSSM), and assess the potential magnitude of the top-quark EDF and WDF in these models, taking into account present experimental constraints. At the end of this section we briefly discuss the potential size of CP-violating form factors in top-quark decay, $t \to Wb$.

3.1 Two-Higgs-doublet models

In view of its large mass the top quark is an excellent probe of non-standard CP violation generated by an extended Higgs sector. We consider here two-Higgs-doublet models (2HDMs) where the SM is extended by an additional Higgs-doublet field and where the Yukawa couplings of the Higgs doublets Φ_1, Φ_2 are such that no tree-level flavour-changing neutral currents (FCNCs) are present. The physical Higgs-boson spectrum of these models consists of a charged Higgs boson and its antiparticle, $H^{\pm}$, and three neutral Higgs bosons, one of which is to be identified with the 125 GeV Higgs resonance. The Higgs potential $V(\Phi_1, \Phi_2)$ can violate CP, either explicitly or spontaneously by Higgs fields developing a vacuum expectation value with non-trivial CP-violating phase. If this is the case, then the physical CP-even and CP-odd neutral Higgs fields mix. In the unitary gauge the resulting three neutral Higgs mass eigenstates h_j are related to the two neutral CP-even states h, H, and the CP-odd state A by an orthogonal transformation:

$$(h_1, h_2, h_3)^T = R\ (h, H, A)^T. \tag{5}$$

The orthogonal matrix R is parametrized by three Euler angles[2] that are related to the parameters of the Higgs potential.

For phenomenological studies it is useful to choose as independent parameters of the 2HDM a set that includes the masses m_j and m_+ of the three neutral and the charged Higgs boson, respectively, the three Euler angles α_i of R, the parameter $\tan\beta = v_2/v_1$ which is the ratio of the vacuum expectation values of the two Higgs-doublet fields, and $\mathrm{v} = \sqrt{v_1^2 + v_2^2}$ which is fixed by experiment to the value $1/\mathrm{v} = (\sqrt{2}G_F)^{1/2} = 246$ GeV. In case of CP violation in the Higgs sector, the Higgs mass eigenstates h_j couple to both scalar and pseudoscalar fermion currents. The Yukawa Lagrangian is

$$\mathcal{L}_Y = -\frac{m_f}{\mathrm{v}}\left(a_{jf}\bar{f}f - b_{jf}\bar{f}i\gamma_5 f\right)h_j. \tag{6}$$

Here f denotes a quark or charged lepton and the reduced scalar and pseudoscalar Yukawa couplings a_{jf}, b_{jf} depend on the type of 2HDM [21], on the matrix elements of R, and on $\tan\beta$.

Within the 2HDM, the CP-violating part of the scattering amplitude of $e^+e^- \to t\bar{t}$ is determined (to one-loop approximation and in the limit of vanishing electron mass m_e) entirely by the top-quark EDF and WDF (4) that are induced at one-loop by CP-violating neutral Higgs-boson exchange [22]. There are no CP-violating box contributions. (A CP-violating scalar form factor $\widetilde{F}_S^Z(s)$ is also generated, but it does not contribute for $m_e = 0$.) Thus the one-loop top-quark EDF and WDF generated in 2HDM are gauge-invariant.

The real and imaginary parts of the top-quark EDF $d_t^{\gamma}(s)$ and WDF $d_t^Z(s)$ were computed for several types of 2HDM in [22]. The EDF $d_t^{\gamma}(s)$ is generated at one loop by the CP-violating exchange of the three Higgs bosons h_j between the outgoing t and $\bar{t}$. A CP-violating Higgs potential implies that

[2] We use the conventions of [20].

the h_j are not mass-degenerate. The form factor becomes complex, i.e., it has an absorptive part for $s > 4m_t^2$. We remark that $d_t^\gamma(s) \propto m_t^3$: two powers of m_t result from the Yukawa interactions (6) and one power from the necessary chirality flip. The one-loop WDF $d_t^Z(s)$ receives two different contributions: the first one is topologically identical to $d_t^\gamma(s)$, but with the tree-level $t\bar{t}$ coupling to the photon replaced by the vectorial $t\bar{t}$ coupling to the Z boson. The second one involves the ZZh_j coupling (where only the CP-even component of h_j is coupled) and the pseudoscalar coupling of h_j to the top quark. The second contribution, which is proportional to $m_Z^2 m_t$, becomes complex for $s > (m_Z + m_j)^2$, where m_j is the mass of h_j.

Before evaluating the formulae for the top-quark EDF and WDF given in [22] we discuss present experimental constraints on the parameters of the type-II 2HDM. The 125 GeV Higgs resonance must be identified with one of the neutral Higgs bosons h_j. For definiteness, we identify it with h_1 and assume the other two neutral Higgs bosons to be heavier. The ATLAS and CMS results on the production and decay of the 125 GeV Higgs resonance $h_1(125\ \text{GeV})$ imply that this boson is Standard-Model like; its couplings to weak gauge bosons, to the t and b quark, and to τ leptons have been determined with a precision of 10–25% [23–25] and these results are in reasonable agreement with the SM predictions. Moreover, the investigation of angular correlations in $h_1(125\ \text{GeV}) \to ZZ^* \to 4\ell$ exclude that this Higgs boson is a pure pseudoscalar ($J^P = 0^-$) [26,27]. However, this does not imply that h_1 is purely CP-even ($J^P = 0^+$) – it can be a CP mixture. Because the pseudoscalar component of such a state does not couple to ZZ and WW at tree level, a potential pseudoscalar component is difficult to detect in the decays of h_1 to weak bosons.[3]

In the following we assume that h_1 is a CP-mixture with couplings to fermions and gauge bosons that are in accord with the LHC constraints [23,24]. We are interested in 2HDM parameter scenarios where the couplings of the h_j to top quarks are not suppressed as compared to the corresponding SM Yukawa coupling. This is the case for $\tan\beta \sim 1$ or somewhat lower than one. Moreover, we assume that the two other neutral Higgs bosons h_2, h_3 are significantly heavier than h_1. In the type-II 2HDM and for $\tan\beta < 1$ the Yukawa couplings of the h_j to b quarks and τ leptons are suppressed as compared to the corresponding SM Yukawa couplings, cf. Table 1. Moreover, the constraint that h_1 has SM-like couplings to weak gauge bosons implies that the couplings of h_2, h_3 to WW and ZZ are small, irrespective of the CP nature of these Higgs bosons. This follows from a sum rule; cf., for instance, [21]. 2HDM parameter scenarios with $\tan\beta \lesssim 1$ and h_2, h_3 masses equal or larger than about 500 GeV are compatible with the non-observation of heavy neutral Higgs bosons at the LHC in final states with electroweak gauge bosons [29–33], b quarks [34,35], charged leptons [36,37], and top quarks [38]. The charged Higgs boson $H^\pm$ of 2HDM is of no concern to us here. Constraints from B-physics data, in particular from the rare decays $B \to X_s + \gamma$ and $B^0 - \bar{B}^0$ mixing imply that the mass of $H^\pm$ must be larger than ~ 700 GeV for low values of $\tan\beta$ [39].

Table 1 Benchmark values of the reduced couplings of the neutral Higgs bosons h_j to quarks, leptons, and weak gauge bosons with $|a_{1t}b_{1t}| \gtrsim 1$ that are in accord with present experimental constraints. The couplings f_{jVV} to the weak gauge bosons are given in units of m_Z^2/v

	a_{jt}	$a_{jb} = a_{j\tau}$	b_{jt}	$b_{jb} = b_{j\tau}$	f_{jVV}
h_1	1.379	0.881	0.910	0.111	0.935
h_2	− 0.569	− 0.275	2.706	0.331	− 0.307
h_3	− 2.634	0.521	− 0.108	0.484	− 0.013

In order to assess the potential size of the form factors $F_{2A}^X(s)$ ($X = \gamma, Z$) in type-II 2HDM with Higgs sector CP violation we make a scan over the independent parameters that are of relevance for this analysis. In the kinematic range $\sqrt{s} \lesssim 500$ GeV the most important contribution to the top-quark EDF and WDF arise from h_1 exchange if this Higgs boson has top-quark Yukawa couplings such that the modulus of the product $a_{1t}b_{1t}$ is about one. We take into account recent constraints on the couplings of h_1 to W, Z, t, b, τ [25] and the experimental constraints on the masses and couplings of h_2, h_3 from Refs. [23,24,29–38]. We vary $\tan\beta$ in the range $0.35 \le \tan\beta \le 1$ and the three Higgs mixing angles in the range $-\pi/2 \le \alpha_i \le \pi/2$, determine the resulting reduced Yukawa couplings a_{jf}, b_{jf} and the couplings f_{jVV} of the h_j to ZZ. A benchmark set of resulting couplings is given in Table 1. Somewhat tighter constraints on the CP-violating top-Higgs couplings were derived in Ref. [40].

For calculating the form factors $F_{2A}^X(s)$ we assume that the Higgs bosons h_2 and h_3 are heavier than 500 GeV. For definiteness we set their masses to be 1200 GeV and 600 GeV, respectively. Using the formulae of Ref. [22], $m_t = 173$ GeV, and the values of the Higgs couplings of Table 1, the real and imaginary parts of $F_{2A}^X(s)$ are shown as functions of the c.m. energy in Fig. 1. In the kinematic range displayed in these plots the imaginary part of the EDF is about three times larger than that of the WDF. This holds true also for the real parts of the form factors close to the $t\bar{t}$ threshold, while they become significantly smaller in magnitude around $\sqrt{s} = 500$ GeV due to the strong fall-off of the dominant contribution from h_1. The values of the real and imaginary parts of these form

[3] The decays $h_1 \to \tau\tau$, where a CP-violating effect occurs at tree level if h_1 is a CP mixture, may be used to check whether or not ϕ_1 has a pseudoscalar component. See, for instance [28]. Other possibilities include the associated production of $t\bar{t}h_1$, once a sufficiently large event sample will have been collected.

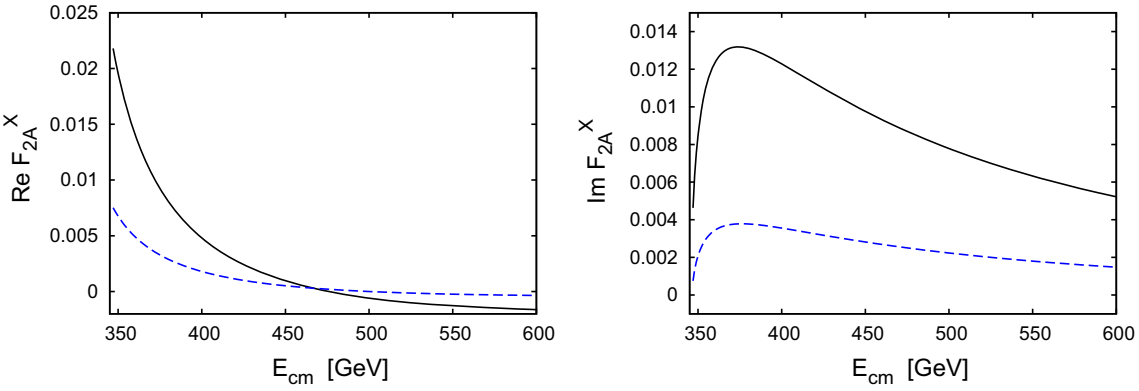

Fig. 1 Left panel: the real part of the top-quark EDF F_{2A}^{γ} (solid, black) and WDF F_{2A}^{Z} (dashed, blue), evaluated with the couplings of Table 1 and neutral Higgs-bosonmasses $m_1 = 125$ GeV, $m_2 = 1200$ GeV, and $m_3 = 600$ GeV, as a function of the c.m. energy. Right panel: the same for the imaginary part of the top-quark EDF and WDF

Table 2 Values of the real and imaginary parts of the top-quark EDF and WDF for two c.m. energies. Input parameters are as in Fig. 1

$\sqrt{s}$ (GeV)	Re F_{2A}^{γ}	Re F_{2A}^{Z}	Im F_{2A}^{γ}	Im F_{2A}^{Z}
380	8.1×10^{-3}	2.9×10^{-3}	1.3×10^{-2}	3.8×10^{-3}
500	-0.6×10^{-3}	0.7×10^{-6}	7.8×10^{-3}	2.2×10^{-3}

factors are listed in Table 2 for two c.m. energies that are chosen for the simulations in Sects. 5–7.

In the kinematic range that we are interested in ($\sqrt{s} \lesssim 500$ GeV) the imaginary parts of the EDF and WDF are rather insensitive to the values of the heavy Higgs-boson masses, as long as $m_{2,3} > 500$ GeV. This is also the case for the real parts of the form factors close to the $t\bar{t}$ threshold that are dominated by the contribution from h_1 exchange. This term falls off strongly with increasing c.m. energy. Moreover, at c.m. energies $\sqrt{s} \gtrsim 500$ GeV the contributions from h_2, h_3 to the real parts of the form factors may no longer be negligible. We find that the real parts of the EDF and WDF at $\sqrt{s} = 500$ GeV depend, for fixed Higgs-boson couplings, sensitively on the masses of h_2, h_3, but do not exceed 10^{-3} in magnitude for the couplings of Table 1.

As mentioned above, the formulae of [22] apply to any type of 2HDM where tree-level FCNC are absent. In fact, the results shown in Fig. 1 and given in Table 2 apply also to other types of 2HDM in the low $\tan\beta$ region; for instance, to the type-I model where all right-chiral quarks and charged leptons are coupled to the Higgs doublet Φ_2 only, or to the so-called lepton specific model where the right-chiral quarks (right-chiral charged leptons) are coupled to Φ_2 (Φ_1) only.

In summary, within the 2HDM the real (imaginary) part of the top-quark electric dipole form factor F_{2A}^{γ} can be as large as ~ 0.02 (~ 0.01) in magnitude near the $t\bar{t}$ production threshold, taking into account the present constraints from LHC data.

3.2 The minimal supersymmetric SM extension

The Higgs sector of the MSSM corresponds to a type-II 2HDM. Supersymmetry (SUSY) forces the tree-level Higgs potential $V(\Phi_1, \Phi_2)$ of the MSSM to conserve CP. Nevertheless, the MSSM contains in its general form many CP-violating phases besides the KM phase, especially in the supersymmetry-breaking terms of the model, including phases of the complex Majorana mass terms of the neutral gauginos and of the complex chargino and sfermion mass matrices. Motivated by assumptions as regards SUSY breaking at very high energies, one often puts constraints on the SUSY-breaking terms, in particular on the CP-violating phases, in order to restrict the number of unknown parameters of the model. Nevertheless, generic features of SUSY CP violation remain. Unlike the case of Higgs-boson induced one-loop EDMs, fermion EDMs generated at one-loop can be large, also for u, d quarks and the electron. The experimental upper bounds on the EDM of the neutron and of atoms/molecules strongly constrain in particular the CP-phases associated with the sfermion mass matrices of the first and second generation, barring fine-tuned cancellations. See, for instance, Ref. [41] for a review. However, the phases of the sfermion mass matrices need not be flavour-universal. For the top flavour the associated phase $\varphi_{\tilde{t}}$ can still be of order one. Often a common phase of the gaugino masses is assumed. Using phase redefinitions of the fields in the MSSM Lagrangian, one can choose for the parametrization of MSSM CP violation in the top-quark sector [42,43] the phase $\varphi_{\tilde{t}}$, the corresponding b-flavour phase $\varphi_{\tilde{b}}$, and the

phase $\varphi_\mu = \arg(\mu)$ of the so-called μ term in the MSSM Lagrangian that generates a Dirac mass of the higgsinos. For a rather recent analysis of constraints on the CP-violating phases in the MSSM, see Ref. [44].

The one-loop top-quark EDF and WDF induced by the CP-violating interactions of the MSSM are gauge-invariant. They are generated by one-loop $\gamma t\bar{t}$ and $Zt\bar{t}$ vertex diagrams involving $\tilde{t}$ and $\tilde{b}$ squarks, gluinos $\tilde{g}$, neutralinos $\tilde{\chi}^0$, and charginos $\tilde{\chi}^\pm$ in the loop. The $\tilde{t}\tilde{t}^*\tilde{g}$ contributions to the EDF and WDF were determined in [45–47]. The complete set of 1-loop contributions were computed in [42,43,48,49]. They consist, apart from the gluino contribution, of the chargino contribution (with $\tilde{\chi}^+\tilde{\chi}^-\tilde{b}$ and $\tilde{b}\tilde{b}^*\tilde{\chi}^+$ in the loop), and of the neutralino contribution (with $\tilde{t}\tilde{t}^*\tilde{\chi}^0$ and $\tilde{\chi}^0\tilde{\chi}^0\tilde{t}$ in the loop).

If light neutralinos and charginos and/or light $\tilde{t}, \tilde{b}$ squarks with masses m_i, m_j of order 100–200 GeV would exist there would be strong enhancements of the top-quark EDF and WDF $F_{2A}^{\gamma,Z}(s)$ in the range $2m_t \lesssim \sqrt{s} \lesssim 500$ GeV near the two-particle production threshold $\sqrt{s}_{th} = m_i + m_j$. References [42,43] computed these form factors for light gauginos and $\tilde{t}, \tilde{b}$ squarks. Reference [43] found maximal values of the form factors at $\sqrt{s} = 500$ GeV for some favourable set of SUSY parameters of the order of 10^{-3}. However, the input parameters of these computations have since been excluded. Searches for supersymmetry were negative so far, and the LHC searches put strong lower bounds on the masses of SUSY particles that are, in most cases, model-dependent, to wit: $m_{\tilde{g}} > 1.8$ TeV, $m_{\tilde{b}_{1,2}} > 840$ GeV, $m_{\tilde{\chi}^\pm} > 715$ GeV, and $m_{\tilde{t}_{1,2}} > 800$ GeV for $m_{\tilde{\chi}_1^0} < 200$ GeV. For a recent review, we refer to Ref. [50]. However, a light stop with mass ~ 200 GeV is not yet excluded if the decay $\tilde{t}_1 \to t\tilde{\chi}_1^0$ exists. The limit $m_{\tilde{\chi}^\pm} > 715$ GeV results from an analysis in Ref. [51] using a simplified SUSY model.

In order to estimate the potential size of the top-quark EDF and WDF, we evaluated the chargino, gluino, and neutralino contributions using the formulae of [42,43] with SUSY masses that are in accord with these experimental constraints. The phases $\varphi_\mu, \varphi_{\tilde{t}}, \varphi_{\tilde{b}}$ were chosen such that they maximize the EDF and WDF for given masses. Using the lower bounds on the masses of SUSY particles cited in the previous paragraph we find

$$\begin{aligned} &|\mathrm{Re}\ F_{2A}^{\gamma}|,\ |\mathrm{Re}\ F_{2A}^{Z}| < 10^{-3}, \\ &|\mathrm{Im}\ F_{2A}^{\gamma}|,\ |\mathrm{Im}\ F_{2A}^{Z}| < 10^{-4} \quad \text{for } \sqrt{s} \lesssim 500\ \text{GeV}. \end{aligned} \tag{7}$$

As mentioned above, a light top squark $\tilde{t}_1$ with mass ~ 200 GeV and a light neutralino $\tilde{\chi}_1^0$ are not yet excluded. In this case non-zero but small imaginary parts are generated by the gluino and neutralino contribution to the EDF and WDF in the considered range of c.m. energies.

In the case of the MSSM there are also CP-violating box contributions to $e^+e^- \to t\bar{t}$ that involve neutralino ($\tilde{e}\tilde{\chi}^0\tilde{\chi}^0\tilde{t}$) and chargino ($\tilde{\nu}_e\tilde{\chi}^\pm\tilde{\chi}^\mp\tilde{b}$) exchanges in the one-loop amplitudes. They are, as shown in [43,49], in general not negligible compared to the top-quark EDF and WDF contributions. We shall, however, refrain from evaluating these box contributions, which goes beyond the scope of this paper. In the simulations performed in Sects. 5–7 we shall stick to the parametrization (1) of CP-violating effects in $t\bar{t}$ production in terms of the EDF and WDF.

3.3 CP-violating form factors in $t \to Wb$

So far, the only top-quark decay mode that has been observed is $t \to Wb$ with subsequent decay of the W boson into leptons or quarks. In the SM the branching ratio of this decay is almost 100%. The decay amplitude for $t \to W^+b$ with all particles on-shell can be parametrized in terms of two chirality-conserving and two chirality-flipping form factors f_L, f_R and g_L, g_R, respectively; cf., for instance, [16]. The measurements of these form factors [52,53] are in agreement with the SM predictions.

Let us denote the corresponding form factors in the charge-conjugate decay $\bar{t} \to W^-\bar{b}$ by f_i', g_i' $(i = L, R)$. CPT invariance implies that $f_i^* = f_i'$ and $g_i^* = g_i'$. CP invariance requires that the corresponding form factors are equal. These relations imply the following: if final-state interactions can be neglected in top-quark decay, then CP violation induces non-zero imaginary parts that are equal in magnitude but differ in sign [16,54]: $\mathrm{Im}\, f_i' = -\mathrm{Im}\, f_i$, $\mathrm{Im} g_i' = -\mathrm{Im} g_i$, $i = L, R$.

In Ref. [54] the potential size of CP-violating (and CP-conserving) contributions to the form factors in $t \to Wb$ was investigated for several SM extensions. Within the 2HDM it was found that $|\mathrm{Im} f_i|, |\mathrm{Im} g_i| \lesssim 3 \times 10^{-4}$ for $\tan\beta \gtrsim 0.6$. In the MSSM the CP-violating effects were found to be smaller by at least one order of magnitude. The observables and CP-violating asymmetries that we introduce in the next section and in Sect. 5 are insensitive to CP violation in top-quark decay. Therefore we can neglect CP violation in top-quark decay in the following and parametrize CP violation in $t\bar{t}$ production with subsequent decay into lepton plus jets final states solely by the top-quark EDF and WDF defined in Eq. (1). One may probe CP violation in semi-leptonic t and $\bar{t}$ decay with a CP-odd asymmetry constructed from suitable triple product correlations [16,46].

3.4 Synopsis

Let us summarize the discussion of the previous subsections. We analyzed the potential size of CP-violating effects in $t\bar{t}$ production in e^+e^- collisions and subsequent t and $\bar{t}$ decay within two popular and motivated SM extensions, taking into account present experimental constraints. As to the BSM scenarios investigated above, an extended Higgs sector with CP-violating neutral Higgs-boson exchange has the largest

potential to generate observable effects in this reaction. If the observed $h_1(125\text{GeV})$ Higgs resonance has both scalar and pseudoscalar couplings to top quarks whose strengths are of order one compared to the SM top Yukawa coupling then the magnitude of Im F_{2A}^{γ} can be $\sim 1\%$ in the energy range $\sqrt{s} \lesssim 500$ GeV that we consider in the following. The real part of this form factor can become of the same order of magnitude near the $t\bar{t}$ threshold. The real and imaginary parts of the top-quark WDF are in general smaller by a factor of about 0.3; cf. Table 2. Within the MSSM the top-quark EDF and WDF are smaller, with maximum values compatible with current experimental constraints below 10^{-3}. The CP-violating form factors in the $t \to Wb$ decay amplitude that can be generated within the 2HDM or the MSSM are very small and of no further interest to us here. Moreover, we recall that within the 2HDM there are no CP-violating box contributions to the $e^+e^- \to t\bar{t}$ amplitude to one-loop approximation if the electron mass is neglected. These results motivate the use of the parametrization of Eq. (1) in the simulations of the following sections.

4 Optimal CP-odd observables

As demonstrated in Ref. [1], at a future linear e^+e^- collider precise measurements of the $t\bar{t}$ cross-section and the top-quark forward–backward asymmetry for two different beam polarizations allow the extraction of the top-quark CP-conserving electroweak form factors with a precision that exceeds that of the HL-LHC. In this section the prospects for the measurement of CP-violating form factors $F_{2A}^{\gamma,Z}$ are investigated, as an extension of the previous study. The CP-violating effects in $e^+e^- \to t\bar{t}$ manifest themselves in specific top-spin effects, namely CP-odd top spin–momentum correlations and $t\bar{t}$ spin correlations. If one considers the dileptonic decay channels, $t\bar{t} \to \ell^+\ell'^- + \cdots$, then it is appropriate to consider CP-odd dileptonic angular correlations [16], which efficiently trace CP-odd $t\bar{t}$ spin correlations. We recall the well-known fact that the charged lepton in semi-leptonic t or $\bar{t}$ decay is by far the best analyzer of the top spin. Here we consider $t\bar{t}$ decay to lepton plus jets final states which yield more events than the dileptonic channels and, moreover, allow for a straightforward experimental reconstruction of the t and $\bar{t}$ rest frames. For these final states the most efficient way to probe for CP-violating effects in $t\bar{t}$ production is to construct observables that result from t and $\bar{t}$ single-spin–momentum correlations, that is, from correlations which involve only the spin of the semi-leptonically decaying t or $\bar{t}$. Here, we adopt the observables proposed in [17] for detecting these correlations in lepton plus jets final states.

We consider in the following the production of a top-quark pair via the collision of longitudinally polarized electron and positron beams:

$$e^+(\mathbf{p}_+, P_{e^+}) + e^-(\mathbf{p}_-, P_{e^-}) \to t(\mathbf{k}_t) + \bar{t}(\mathbf{k}_{\bar{t}}). \tag{8}$$

Here, $\mathbf{p}_\pm$ and $\mathbf{k}_t, \mathbf{k}_{\bar{t}}$ denote the $e^\pm$, t, and $\bar{t}$ three-momenta in the e^+e^- c.m. frame. The spin degrees of freedom of the t and $\bar{t}$ are not exhibited. Moreover, P_{e^-} (P_{e^+}) is the longitudinal polarization degree of the electron (positron) beam. In our notation, $P_{e^-} = -1$ ($P_{e^+} = -1$) refers to left-handed electrons (positrons). For our purpose the most useful final states are, as mentioned, the lepton plus jets final states from semi-leptonic t decay and hadronic $\bar{t}$ decay and vice versa:

$$t\ \bar{t} \to \ell^+(\mathbf{q}_+) + \nu_\ell + b + \overline{X}_{\text{had}}(\mathbf{q}_{\bar{X}}), \tag{9}$$

$$t\ \bar{t} \to X_{\text{had}}(\mathbf{q}_X) + \ell^-(\mathbf{q}_-) + \bar{\nu}_\ell + \bar{b}, \tag{10}$$

where the three-momenta in (9) and (10) also refer to the e^+e^- c.m. frame.

We compute the reactions (8)–(10) at tree level, both in the SM and with non-zero CP-odd form factors $F_{2A}^{\gamma,Z}$, taking the polarizations and spin correlations of the intermediate t and $\bar{t}$ into account. As discussed in the previous section these form factors can have imaginary parts. Non-zero real parts $\text{Re}\,F_{2A}^{\gamma,Z}(s)$ induce a difference in the t and $\bar{t}$ polarizations orthogonal to the scattering plane of the reaction. Non-zero absorptive parts, $\text{Im}\,F_{2A}^{\gamma,Z}(s)$, lead to a difference in the t and $\bar{t}$ polarizations along the top-quark direction of flight and along the direction of the electron or positron beam. At the level of the intermediate t and $\bar{t}$ these effects manifest themselves in non-zero expectation values of the following CP-odd observables:

$$\left(\hat{\mathbf{p}}_+ \times \hat{\mathbf{k}}_t\right) \cdot (\mathbf{s}_t - \mathbf{s}_{\bar{t}}), \quad \hat{\mathbf{k}}_t \cdot (\mathbf{s}_t - \mathbf{s}_{\bar{t}}), \quad \hat{\mathbf{p}}_+ \cdot (\mathbf{s}_t - \mathbf{s}_{\bar{t}}), \tag{11}$$

where $\mathbf{s}_t$ and $\mathbf{s}_{\bar{t}}$ denote the spin operators of t and $\bar{t}$, respectively, and hats denote unit vectors. In (11) two-body kinematics is used, i.e., $\mathbf{k}_{\bar{t}} = -\mathbf{k}_t$. The expectation value of the first observable of the list (11) depends on $\text{Re}\,F_{2A}^{\gamma,Z}$, while the expectation values of the other two observables depend on $\text{Im}\,F_{2A}^{\gamma,Z}$. Each observable listed in (11) is the difference of two terms that involve the t and $\bar{t}$ spin, respectively. The term that contains the t ($\bar{t}$) spin can be translated, in the case of the lepton plus jets final states, into a correlation that involves the ℓ^+ (ℓ^-) direction of flight. This is the most efficient way to analyze the t ($\bar{t}$) spin. These correlations can be measured with the ℓ^+ + jets and ℓ^- + jets events (9) and (10), respectively.

Based on these considerations, so-called optimal observables [15], i.e., observables with a maximal signal-to-noise ratio to a certain parameter appearing in the squared matrix element, were constructed in Ref. [17] for tracing CP violation in the lepton plus jets final states (9) and (10). These optimal observables are, in essence, given by those parts of the squared matrix element that are linear in the CP-violating form factors $\text{Re}\,F_{2A}^{\gamma,Z}$ or $\text{Im}\,F_{2A}^{\gamma,Z}$. One may simplify these

expressions and use for the final states (9) the following two observables [17] that are nearly optimal:

$$\mathcal{O}_+^{Re} = (\hat{\mathbf{q}}_{\bar{X}} \times \hat{\mathbf{q}}_+^*) \cdot \hat{\mathbf{p}}_+, \tag{12}$$

$$\mathcal{O}_+^{Im} = -\left[1 + \left(\frac{\sqrt{s}}{2m_t} - 1\right)(\hat{\mathbf{q}}_{\bar{X}} \cdot \hat{\mathbf{p}}_+)^2\right] \hat{\mathbf{q}}_+^* \cdot \hat{\mathbf{q}}_{\bar{X}} + \frac{\sqrt{s}}{2m_t} \hat{\mathbf{q}}_{\bar{X}} \cdot \hat{\mathbf{p}}_+ \hat{\mathbf{q}}_+^* \cdot \hat{\mathbf{p}}_+. \tag{13}$$

The corresponding observables $\mathcal{O}_-$ for the final states (10) are defined to be the CP image of $\mathcal{O}_+$ and are obtained from $\mathcal{O}_+$ by the substitutions $\hat{\mathbf{q}}_{\bar{X}} \to -\hat{\mathbf{q}}_X$, $\hat{\mathbf{q}}_+^* \to -\hat{\mathbf{q}}_-^*$, $\hat{\mathbf{p}}_+ \to \hat{\mathbf{p}}_+$. The unit vectors $\hat{\mathbf{q}}_\pm^*$ refer to the $\ell^\pm$ directions of flight defined in the t and $\bar{t}$ rest frame, respectively. The differences of the expectation values of $\mathcal{O}_+$ and $\mathcal{O}_-$ that we consider in the next section probe for CP-violating effects.

The observables (12) and (13) are approximations to the rather unwieldy optimal observables listed in the appendix of Ref. [17]. Using the optimal observables at low energy leads to a minor increase in sensitivity. Between the $t\bar{t}$ production threshold and $\sqrt{s} \sim 500$ GeV the sensitivity to the CP-odd form factors increases by a few percent. At very high energy the difference is somewhat more pronounced: at 3 TeV the sensitivity is expected to increase by approximately 30%.

As discussed in Sect. 3.3, non-standard CP-violating interactions can induce, besides CP violation in $t\bar{t}$ production, also anomalous couplings in the $t \to W^+ b$ and $\bar{t} \to W^- \bar{b}$ decay amplitudes. However, observables such as (12) and (13) and their CP images, where the t and $\bar{t}$ spins are analyzed by charged lepton angular correlations, are insensitive to these anomalous couplings, as long as one uses the linear approximation [46,55,56] which is legitimate here. This justifies the parametrization of the CP asymmetries $\langle \mathcal{O}_+ \rangle - \langle \mathcal{O}_- \rangle$ solely in terms of $F_{2A}^{\gamma,Z}$.

5 Polarized beams

We study the distributions of $\mathcal{O}_-^{Re}$ and $\mathcal{O}_-^{Im}$ at leading-order (LO) in the SM couplings, putting $F_{2A}^{\gamma,Z} = 0$, with the WHIZARD 1.95 event generator [57]. Distributions of both observables are shown in Fig. 2 for a centre-of-mass energy of 500 GeV. The three histograms in each panel correspond to unpolarized beams (dashed line), to a left-handed electron beam and a right-handed positron beam ($e_L^- e_R^+$, $P_{e^-}, P_{e^+} = -80\%, +30\%$, red continuous histogram) and for a right-handed electron beam and a left-handed positron beam ($e_R^- e_L^+$, $P_{e^-}, P_{e^+} = +80\%, -30\%$, black continuous histogram). The degree of longitudinal polarization that is used follows the design values of the ILC: $P_{e^-}, P_{e^+} = \pm 80\%, \mp 30\%$. As the top-quark EDF and WDF are negligible in the SM (and set to zero in the simulation), the distributions for unpolarized beams are symmetric around the origin.

Initial-state polarization affects the normalization, but leaves the shape of the $\mathcal{O}_-^{Re}$ distribution unaffected. The total cross-section increases strongly for e^+e^- beams in the $e_L^- e_R^+$ configuration as compared to unpolarized beams, and somewhat less strongly for the polarization configuration $e_R^- e_L^+$.

Beam polarization has a more profound impact on $\mathcal{O}_-^{Im}$ as shown in Fig. 2 (right panel). With unpolarized beams the distribution is symmetric around zero, but the distributions corresponding to polarized beams show significant distortions. This is expected because the initial state with different beam polarization for electrons and positrons is not CP-symmetric.

Asymmetries $\mathcal{A}$ can be defined [17] as the difference of the expectation values $\langle \mathcal{O}_+ \rangle$ and $\langle \mathcal{O}_- \rangle$:

$$\mathcal{A} = \langle \mathcal{O}_+(s, \hat{\mathbf{q}}_+^*, \hat{\mathbf{q}}_{\bar{X}}, \hat{\mathbf{p}}_+) \rangle - \langle \mathcal{O}_-(s, \hat{\mathbf{q}}_-^*, \hat{\mathbf{q}}_X, \hat{\mathbf{p}}_+) \rangle. \tag{14}$$

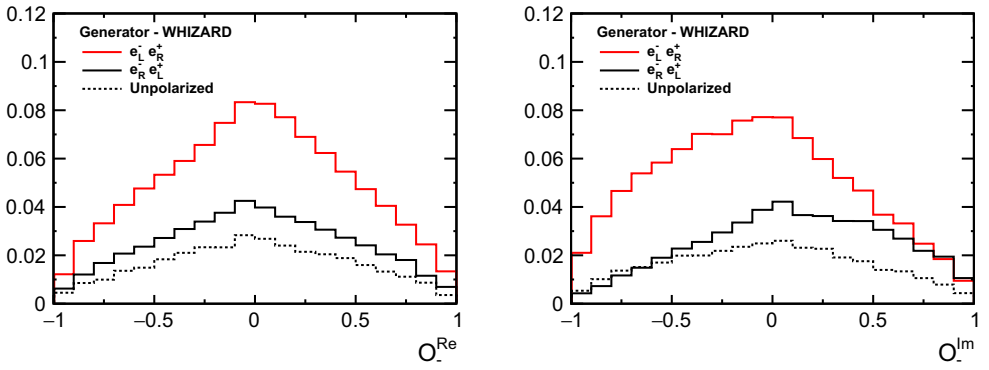

Fig. 2 The WHIZARD LO Standard Model prediction for the normalized distribution of the CP observables $\mathcal{O}_-^{Re}$ (left panel) and $\mathcal{O}_-^{Im}$ (right panel) defined in (12) and (13). The results correspond to e^+e^- collisions at a centre-of-mass energy of 500 GeV and three different beam polarizations: the dashed line corresponds to unpolarized beams, the red (black) solid lines to − 80% (+ 80%) polarization of the electron beam and + 30% (− 30%) polarization of the positron beam. The histogram for LR polarized beams is normalized to unit area. The area of the other histograms is scaled so as to maintain the cross-section ratios. The $\mathcal{O}_\pm^{Re}$ distribution is confined to $[-1, 1]$ by construction, the $\mathcal{O}_\pm^{Im}$ distribution is truncated to the same interval

Table 3 The values of the coefficients in the expressions for the asymmetries $\mathcal{A}^{Re}$ and $\mathcal{A}^{Im}$. The values are calculated for several c.m. energies used in this paper and for the $e^-_L e^+_R$ beam-polarization configuration ($P_{e^-} = -1$, $P_{e^+} = +1$)

c.m. energy $\sqrt{s}$ (GeV)	$c_\gamma(s)$	$c_Z(s)$	$\tilde{c}_\gamma(s)$	$\tilde{c}_Z(s)$
380	0.245	0.173	0.232	0.164
500	0.607	0.418	0.512	0.352
1000	1.714	1.151	1.464	0.983
1400	2.514	1.681	2.528	1.691
3000	5.589	3.725	10.190	6.791

Table 4 Same as Table 3, but for the opposite $e^-_R e^+_L$ beam polarization: $P_{e^-} = +1$, $P_{e^+} = -1$

c.m. energy $\sqrt{s}$ (GeV)	$c_\gamma(s)$	$c_Z(s)$	$\tilde{c}_\gamma(s)$	$\tilde{c}_Z(s)$
380	− 0.381	0.217	0.362	− 0.206
500	− 0.903	0.500	0.761	− 0.422
1000	− 2.437	1.316	2.081	− 1.124
1400	− 3.549	1.909	3.569	− 1.920
3000	− 7.845	4.205	14.302	− 7.667

In the asymmetry, many experimental effects are expected to cancel. This applies also to the distortion of the $\mathcal{O}^{Im}_{\pm}$ distributions by beam polarization. The $\mathcal{O}^{Im}_{+}$ and $\mathcal{O}^{Im}_{-}$ distributions are shifted by approximately equal amounts, but in opposite directions. The mean value of the $\mathcal{O}^{Im}_{-}$ observable is − 0.08 ± 0.01 for P_{e^-}, $P_{e^+} = -80\%, +30\%$ and + 0.09 ± 0.01 for P_{e^-}, $P_{e^+} = +80\%, -30\%$. The distributions of $\mathcal{O}^{Im}_{+}$ are distorted in the same way as those of $\mathcal{O}^{Im}_{-}$. Therefore, the effect of initial-state polarization cancels in the difference of the two observables.

The asymmetries $\mathcal{A}^{Re}$, $\mathcal{A}^{Im}$ are sensitive to CP violation effects in the $t\bar{t}$ production amplitude through the contributions of $\mathrm{Re}F^{\gamma,Z}_{2A}$ and $\mathrm{Im}F^{\gamma,Z}_{2A}$, respectively:

$$\mathcal{A}^{Re} = \langle \mathcal{O}^{Re}_{+} \rangle - \langle \mathcal{O}^{Re}_{-} \rangle = c_\gamma(s)\mathrm{Re}F^{\gamma}_{2A} + c_Z(s)\mathrm{Re}F^{Z}_{2A}, \tag{15}$$

$$\mathcal{A}^{Im} = \langle \mathcal{O}^{Im}_{+} \rangle - \langle \mathcal{O}^{Im}_{-} \rangle = \tilde{c}_\gamma(s)\mathrm{Im}F^{\gamma}_{2A} + \tilde{c}_Z(s)\mathrm{Im}F^{Z}_{2A}. \tag{16}$$

The values of these coefficients depend on the polarizations P_{e^-} and P_{e^+}. In our approach, where we normalize the expectation values $\langle \mathcal{O} \rangle$ by the SM cross section (that is, neglecting the contributions bilinear in the CP-violation form factors), the asymmetries $\mathcal{A}^{Re}$, $\mathcal{A}^{Im}$ are strictly linear in the form factors. Analytical expressions for the coefficients $c_\gamma(s)$, $c_Z(s)$, $\tilde{c}_\gamma(s)$ and $\tilde{c}_Z(s)$ of relations (15) and (16) for arbitrary beam polarization are given in the appendix. Values for 100% polarization are given in Tables 3 and 4, using $m_t = 173.34$ GeV, $m_Z = 91.1876$ GeV, $m_W = 80.385$ GeV, and $\sin^2\theta_W = 1 - m^2_W/m^2_Z$.

The polarization of the e^- and e^+ beams provides a means to disentangle the contributions of the CP-violating photon and Z-boson vertices. The coefficients $c_\gamma(s)$ and $\tilde{c}_Z(s)$ corresponding to the LR and RL configurations have opposite signs. The measurement of the two CP asymmetries $\mathcal{A}^{Re}$ and $\mathcal{A}^{Im}$ for two beam polarizations provides sufficient constraints to solve the system of equations formed by Eqs. (15) and (16).

For $\sqrt{s} \gg 2m_t$ the coefficients $c_\gamma(s)$, $c_Z(s)$ that appear in the expression for $\mathcal{A}^{Re}$ grow with the c.m. energy $\sqrt{s}$. The interactions associated with $F^{\gamma,Z}_{2A}$ involve a factor k^ν, which is the sum of the t and $\bar{t}$ four-momenta (cf. Eq. (1)). Therefore, the sensitivity of the asymmetry $\mathcal{A}^{Re}$ to F_{2A} increases with centre-of-mass energy.

The observables $\mathcal{O}^{Im}_{\pm}$ consist of a sum of terms, two of which contain the factor $\sqrt{s}$. Therefore the coefficients $\tilde{c}_\gamma(s)$, $\tilde{c}_Z(s)$ that determine $\mathcal{A}^{Im}$ grow with s for $\sqrt{s} \gg 2m_t$. However, this does not imply that this asymmetry has a significantly higher sensitivity than $\mathcal{A}^{Re}$ to CP-violating effects in $t\bar{t}$ production at high energies, because the widths of the distributions of $\mathcal{O}^{Im}_{\pm}$ grow accordingly.

6 Full simulation: ILC at 500 GeV

In this section we study the 500 GeV run of the ILC, assuming an integrated luminosity of 500 fb^{-1}. The sample is divided into two beam-polarization configurations: the LR sample has − 80 and + 30% electron and positron polarization, respectively. In the RL sample the signs of both electron and positron polarization are inverted: the electron polarization is + 80% and the positron polarization is − 30%.

The full-simulation study is based on samples produced for the ILC TDR [58]. The event sample is generated with WHIZARD 1.95 [59] by the LCC generator group. It includes all six-fermion processes that produce a lepton plus jets final state, $e^+e^- \to b\bar{b}l^\pm\nu_l q\bar{q}$. This includes top-quark pair production and a number of other processes that lead to the same final state, with the largest non-doubly-resonant contribution coming from single-top production [60]. The effect of initial-state radiation (ISR) is included in the generator. Events are generated with the nominal ILC luminosity spectrum described in Ref. [58], which includes the effects of beam energy spread and beamstrahlung. The events generated are restricted to the physics of the SM, hence the $F^{\gamma,Z}_{2A}$ are set to zero. Fragmentation and hadronization is modelled using PYTHIA 6.4 [61] with a parameter set tuned to e^+e^- data recorded at LEP.

The generated events are processed with the ILD detector simulation software based on GEANT4 [62]. The ILD detector model is described in the *Detailed Baseline Design* included in the ILC TDR [58]. The ILD detector consists of cylindrical *barrel* detectors and two *end-caps*. Together these

provides nearly hermetic coverage down to a polar angle of approximately 6 degrees. For the reconstruction of charged particles ILD relies on a combination of a solid and gaseous tracking system in a 3.5 Tesla magnetic field. Precise silicon pixel and micro-strip detectors occupy the inner radii, from $r = 1.5$ cm to $r = 33$ cm. A large Time Projection Chamber provides measurements out to 1.8 m. The tracker is surrounded by a highly granular calorimeter designed for particle flow. A highly segmented tungsten electromagnetic calorimeter provides up to 30 samples in depth with a transverse cell size of 5×5 mm^2. This is followed by a highly segmented hadronic calorimeter with 48 steel absorber layers and 3×3 cm^2 read-out tiles.

The $\gamma\gamma \to$ *hadrons* background corresponding to a single bunch crossing is overlaid. The data from the different subdetectors are combined into particle-flow objects (PFO) using the Pandora [63] particle-flow algorithm. Jets are reconstructed using a robust algorithm [64] specifically designed for high-energy lepton colliders with non-negligible background levels. Particle-flow objects are clustered into exactly four jets. Heavy-flavour jets are identified using the LCFI algorithm [65,66].

The selection and reconstruction of the top-quark candidates proceeds as described in Ref. [1]. The event selection relies primarily on the presence of the b-jets and the lepton from the W-boson decay.

Leptons are identified by the particle-flow algorithm. A number of criteria is applied to the lepton and the jet containing the lepton to ensure that the lepton is isolated: the ratio p_T^l/M_j of the lepton p_T and the invariant mass of the jet must be greater than 0.25. The energy of the lepton must be greater than 60% of the jet energy. Exactly one isolated lepton must be present in the event. The isolated lepton is removed from the collection of particle-flow objects and jet clustering is repeated on the remaining objects.

The LCFI flavour tagger returns a likelihood for the four reconstructed jets, that is, based on track and vertex information. At least one jet must satisfy a stringent requirement (b-tag likelihood greater than 0.9). A second jet must be found in the event that satisfies a looser requirement (b-tag likelihood greater than 0.6).

After these basic requirements the non-$WbWb$ background is reduced to a manageable level. No strong cuts on kinematic observables are required to isolate the signal. A number of loose cuts are applied to the invariant mass of the hadronic final state ($180 < m_{\text{had.}} < 420$ GeV) and on the mass of the reconstructed W-bosons and top quarks ($120 < m_W < 250$ GeV and $120 < m_t < 270$ GeV. These have virtually no effect on the signal selection efficiency, but are helpful to reduce the background due to two-fermion and four-fermion events.

The $e^+e^- \to b\bar{b}l^\pm\nu_l q\bar{q}$ process includes a small fraction of single top, which is considered part of the signal, and less than 1% of WWZ events. The selection is based on extensive studies in Refs. [1,67]. The contamination of the signal sample by events due to processes other than those included in the $e^+e^- \to b\bar{b}l^\pm\nu_l q\bar{q}$ sample is less than 5% and is neglected in the following.

The average selection efficiency for signal events is approximately 54% for the LR sample and 56% for the RL polarized case. The efficiency is over 70% for events with muons and 2% lower for events with electrons or positrons. Events with τ-leptons enter the signal selection with an efficiency of 20%, thanks to τ-decays to electrons and muons. As expected, no significant difference is observed between the selection efficiencies for positively and negatively charged leptons.

The hadronic top candidate is reconstructed by pairing the two light-quark jets with the b-jet that minimizes a χ^2 based on the expected W-boson and top quark energy and mass and on the angle between the W-boson and the b-jet. For $e_L^- e_R^+$ polarization migrations strongly affect the distributions. A maximum χ^2 is required to retain only well-reconstructed events. This requirement reduces the overall selection efficiency to approximately 30%. This quality cut is not applied for $e_R^- e_L^+$ polarization, where migrations have a small effect.

The reconstructed distributions for the observables $\mathcal{O}_\pm^{Re}$ and $\mathcal{O}_\pm^{Im}$ are shown in Fig. 3. In the same figure the true distribution is shown, that is, the distribution of the observable constructed with the lepton and top quark from the Monte Carlo record, before any detector effects or selection cuts are applied.

The event selection has a clear impact on the distributions of $\mathcal{O}_\pm^{Re}$. A dip in the central part of the reconstructed distributions is observed that is due to the limited acceptance of the experiment in the forward region. The cuts on lepton energy and isolation have a very small effect. The energy resolution of the reconstructed hadronic top-quark candidate and ambiguities in the assignment of b-jets to W-boson candidates leads to a slight broadening of the distribution. The distributions of $\mathcal{O}_\pm^{Im}$, moreover, exhibit the expected asymmetry due to the beam polarization.

The response of the experiment is the same for positively and negatively charged leptons and for the hadronic top and anti-top quark decay products. Therefore, any distortions in the reconstructed distributions are expected to cancel in the asymmetries $\mathcal{A}^{Re}$ and $\mathcal{A}^{Im}$. Experimental effects generally do not generate spurious asymmetries. The reconstructed asymmetries in Table 5 are found to be compatible with zero within the statistical uncertainty of 0.003–0.004.

7 Full simulation: CLIC at 380 GeV

In this section we study the potential of CLIC operation at $\sqrt{s} = 380$ GeV. The baseline CLIC design allows for up

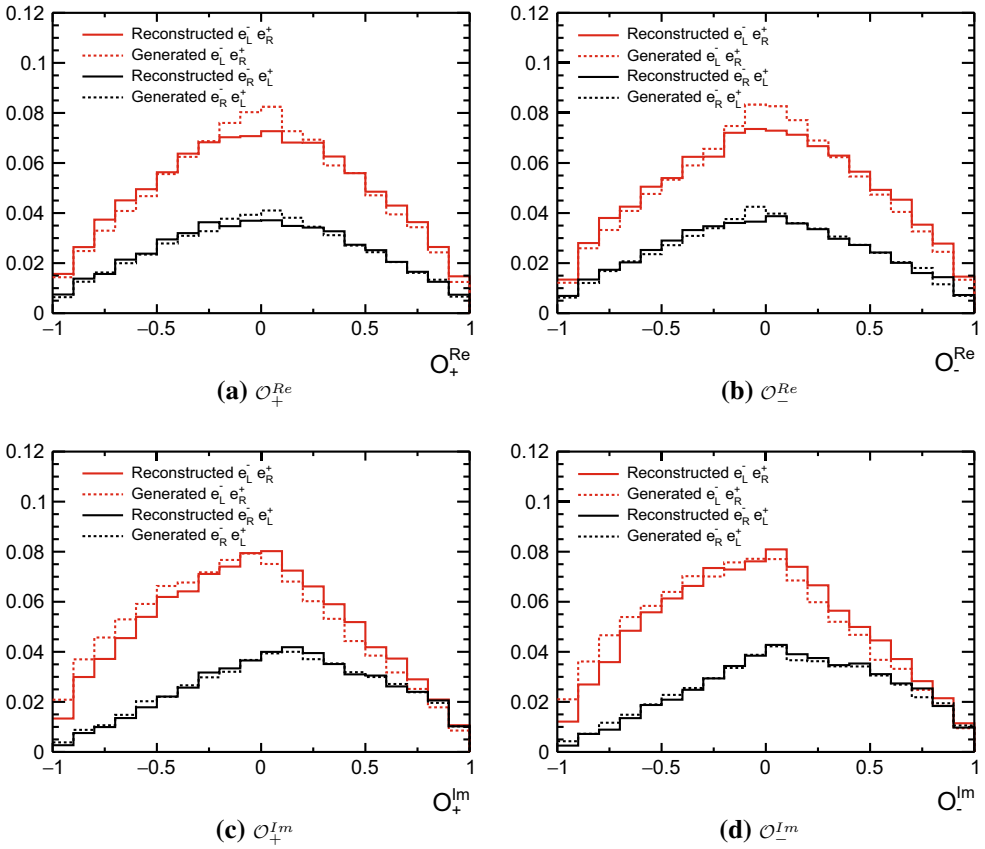

(a) $\mathcal{O}^{Re}_+$ **(b)** $\mathcal{O}^{Re}_-$ **(c)** $\mathcal{O}^{Im}_+$ **(d)** $\mathcal{O}^{Im}_-$

Fig. 3 The CP-odd observables $\mathcal{O}^{Re,Im}_{\pm}$ for the ILC at $\sqrt{s} = 500$ GeV. The four distributions correspond to the reconstructed (solid) and true (dashed) distributions for two beam polarizations. The red histogram $(e^-_L e^+_R)$ corresponds to -80% electron polarization and $+30\%$ positron polarization, theblack histogram $(e^-_R e^+_L)$ to $+80\%$ electron polarization and -30% positron polarization. The histogram for the left-handed electron beam is normalized to unit area. The area of the histogram for right-handed polarization is scaled so as to maintain the cross section ratios

Table 5 Reconstructed values of the CP-odd asymmetries from a Monte Carlo simulation of the ILD detector response to $t\bar{t}$ events produced in electron–positron collisions at $\sqrt{s} = 500$ GeV. The quoted uncertainties are due to the limited statisitcs of the simulated samples

Polarization	$e^-_L e^+_R$ $(P_{e^-}, P_{e^+} = -0.8, +0.3)$	$e^-_R e^+_L$ $(P_{e^-}, P_{e^+} = +0.8, -0.3)$
$\mathcal{A}^{Re}$	-0.001 ± 0.003	-0.009 ± 0.004
$\mathcal{A}^{Im}$	0.0004 ± 0.003	-0.005 ± 0.004

to $\pm$ 80% longitudinal electron polarization ($P_{e^-} = \pm 0.8$). Space is reserved in the layout for positron polarization as an upgrade option. No positron polarization is assumed in the following. An integrated luminosity of 500 fb^{-1} is assumed.

Events are generated with WHIZARD 1.95 [59], again including all six-fermion processes that produce the relevant final state. The effect of ISR and the CLIC luminosity spectrum are taken into account. The machine parameters correspond to the settings reported in the CLIC Conceptual Design Report [10].

The generated events are processed with a full simulation of the CLIC_ILD detector [10]. The CLIC_ILD detector is an adaptation of the ILD detector described in Sect. 6 to the high-energy environment. To deal with machine-induced backgrounds the vertex detector is moved out to $r = 2.5$ cm and the time stamping capabilities of the detector are reinforced. The thickness of the calorimeter is enhanced to fully contain energetic jets: the combination of electromagnetic and hadronic systems corresponds to 8.5 interaction lengths. The electromagnetic calorimeter and barrel hadron calorimeter use Tungsten as absorber material. The end-cap has iron absorber layers. The electromagnetic calorimeter is read out by 30 sampling layers with finely segmented silicon detectors, with a pad size of 5×5 mm^2. The hadronic calorimeter is read out by 75 layers (60 in the end-cap) of scintillator material with a cell size of 30×30 mm^2.

To deal with the background from $\gamma\gamma \rightarrow$ *hadrons*, particle-flow objects are selected using a set of timing and energy cuts, corresponding to the loose selection of Ref. [68].

The event selection is identical to that described in Sect. 6. The b-tagging likelihood cut is reoptimized to achieve a simi-

Table 6 Reconstructed values of the CP-odd asymmetries from a Monte Carlo simulation of the CLIC_ILD detector response to $t\bar{t}$ events produced in electron–positron collisions at $\sqrt{s} = 380$ GeV. The quoted uncertainties are due to the limited statisitcs of the simulated samples

Polarization	e^-_L ($P_{e^-} = -0.8$)	e^-_R ($P_{e^-} = +0.8$)
$\mathcal{A}^{Re}$	-0.001 ± 0.003	0.009 ± 0.004
$\mathcal{A}^{Im}$	0.0003 ± 0.003	-0.002 ± 0.003

lar signal efficiency. The overall selection efficiency is somewhat higher than for the ILC at 500 GeV: 58% for the average over lepton flavours and beam polarizations. The efficiencies for the two beam polarizations agree within 1%. A similar pattern is observed for the lepton flavours: the efficiency for events with muons, electrons and τ-leptons are ~ 82, ~ 74 and $\sim 20\%$.

Reconstruction of the W-boson and top quark candidates proceeds as described in Sect. 6. At a centre-of-mass energy of 380 GeV the observables are reconstructed quite accurately. The distributions are centered at zero. A slight dip is visible at the centre of the reconstructed $\mathcal{O}^{Re}_{\pm}$ distribution due to the limited acceptance in the forward region of the experiment. Other than that, the differences between reconstructed and generated distributions are very small.

Again, we find that the reconstructed asymmetries given in Table 6 are compatible with zero within the statistical uncertainty. The entry of $\mathcal{A}^{Re}$ for $P_{e^-} = +0.8$, that is, 2 σ away from 0, is taken to be a statistical fluctuation. Studies of selection and reconstruction at parton level with much larger samples fail to generate spurious non-zero values for the asymmetry. Higher-order QCD corrections to continuum $t\bar{t}$ production and decay are known to be moderate to small (cf. the brief discussion in Sect. 9, where references are given). Therefore we expect that these corrections affect the shape of the distributions of the observables $\mathcal{O}^{Re}_{\pm}$, $\mathcal{O}^{Im}_{\pm}$ (Figs. 3 and 4), presented in this and in the previous section, only in a rather moderate way. Much more important are the experimental effects of limited acceptance, efficiency, and bin migration on the shape of these distributions, discussed in Sect. 9. Moreover, the QCD corrections (which are, needless to say, CP-invariant) cancel in the CP-odd asymmetries $\mathcal{A}^{Re}$ and $\mathcal{A}^{Im}$. Only a small residual effect remains via the effect of the QCD corrections on the normalization of the expectation values that enter these asymmetries. We will estimate the resulting theoretical uncertainties in Sect. 9.

8 Parton-level study for high-energy operation

In this section we study the potential of the high-energy stages of the CLIC programme that could reach 3 TeV. The instantaneous luminosity scales approximately proportional to the centre-of-mass energy and one may expect an integrated luminosity of several ab^{-1}.

The decay of boosted top quarks produces a topology [69] that is very different from that of $t\bar{t}$ events close to the production threshold. Therefore, the reconstruction of the 1–3 TeV collisions must be performed with an algorithm specifically developed for high energy, where the collimated decay products of the hadronic top quark are captured in a single large-R jet (i.e. a jet reconstructed with a radius parameter R greater than 1). In this reconstruction scheme the combinatoric problem of pairing W-boson and b-tagged jets is entirely avoided.

The $\gamma\gamma \to hadrons$ background in multi-TeV collisions is more severe than at low energy. The reconstruction of boosted top quarks at CLIC was studied in a detailed simulation, including realistic background levels in Ref. [70]. With tight pre-selection cuts on the particle-flow objects and the robust algorithm of Ref. [64] the top-quark energy can be reconstructed with a resolution of 8%. Also the jet mass and other substructure observables can be reconstructed precisely, with much better resolution than at the LHC. As background processes have cross-sections that are similar to that of top-quark production, it seems safe to assume that $t\bar{t}$ events with centre-of-mass energies of 1–3 TeV can be efficiently selected and distinguished from background processes.

An evaluation based on a detailed simulation of the experimental response for the optimal observables is not yet available. We identify the most important effects using a parton-level simulation. A representative selection is applied to parton-level $e^+e^- \to t\bar{t} \to b\bar{b}q\bar{q}'l\nu$ events generated with MG5_aMC@NLO [71]. The detector resolution is implemented by smearing of the parton four-vectors.

The limited acceptance in the forward region shapes the distributions significantly. For partons emitted at shallow angle, part of the jet energy flow disappears down the beam pipe. We mimic this effect by requiring that all partons have $|\cos\theta| < 0.98$ (the detector coverage extends to well beyond $|\cos\theta| = 0.99$; some margin is added as jets have a finite size). In Fig. 5 the distribution for selected events is compared to the full distribution. The effect is more pronounced and more localized than in the low-energy analysis.

We furthermore apply a smearing to mimic the resolution for the hadronic top quark candidate. The reconstructed top-quark four-vector is used to boost the lepton to the top-quark system. The finite energy resolution and angular resolution may lead to distortions of the reconstructed distribution. The effects of a 10% energy resolution and 0.02 radian angular resolution, twice the size of the resolution found in the study of Ref. [70], are indicated in Fig. 5. The reconstruction has a much less severe impact than in the low-energy analysis.

As for the low-energy analysis, these experimental effects are identical for positively and negatively charged leptons and for quarks and anti-quarks. We therefore expect that exper-

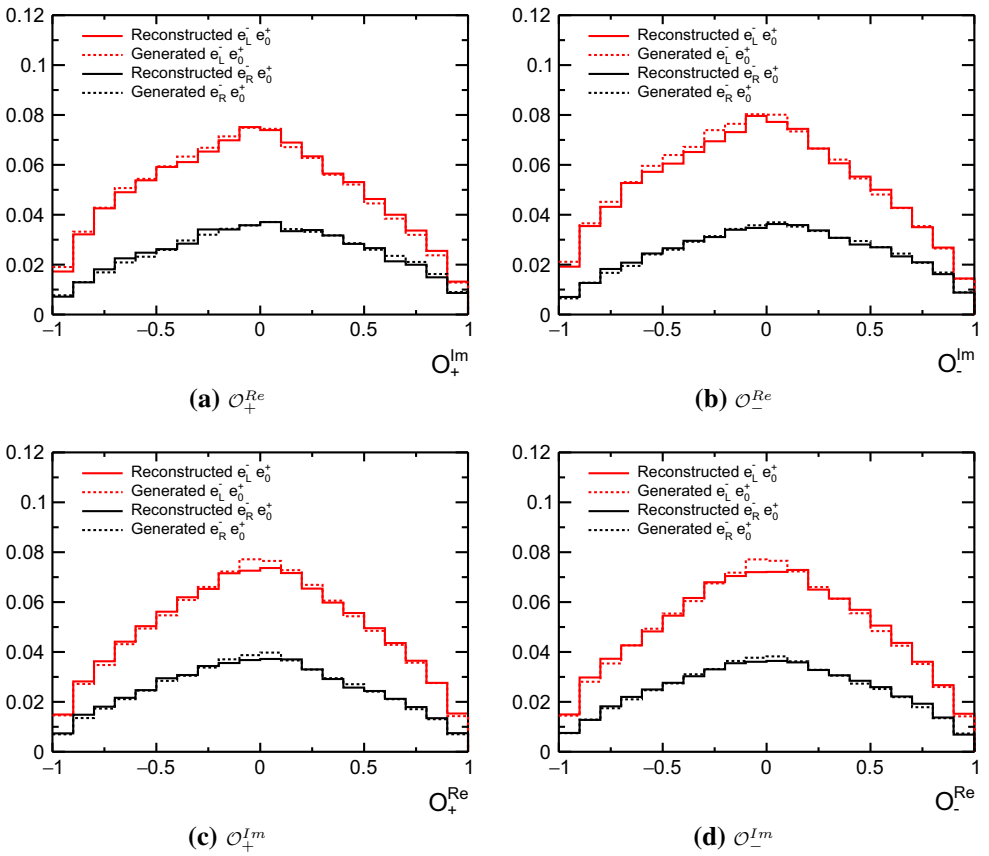

(a) $\mathcal{O}_+^{Re}$ **(b)** $\mathcal{O}_-^{Re}$

(c) $\mathcal{O}_+^{Im}$ **(d)** $\mathcal{O}_-^{Im}$

Fig. 4 The CP-odd observables $\mathcal{O}_\pm^{Re,Im}$ for CLIC at $\sqrt{s} = 380$ GeV. The four distributions correspond to the reconstructed and true distributions for two beam polarizations. The red histogram $(e_L^- e_0^+)$ corresponds to − 80% electron polarization, the blackhistogram $(e_R^- e_0^+)$ to + 80% electron polarization. The histogram for the left-handed electron beam is normalized to unit area. The area of the histogram for right-handed polarization is scaled so as to maintain the cross-section ratios

imental effects do not create spurious asymmetries. Rough, but conservative, limits on systematic effects are presented in the next section.

A more detailed study of a detailed detector simulation is required for a quantitative study of the high-energy performance. In the following we estimate the potential of high-energy operation, assuming an acceptance of 40% for lepton + jets events.

9 Systematic uncertainties

Before we discuss the prospects of linear colliders to extract the real and imaginary parts of the form factors $F_{2A}^{\gamma,Z}$, a number of potential sources of systematic uncertainties are briefly discussed.

The polarization of the electron and positron beams is the key machine parameter in the extraction of the form factors. A combination of polarimeters and in-situ measurements allows for a precise determination of P_{e^-} and P_{e^+}. The detailed study of the ILC case in Ref. [72] envisages a determination to the 10^{-3} level. The study of (single) W-boson production is expected to provide per-mille level precision at high energy. This precision is well beyond what is needed to avoid significant uncertainties in the form factor extraction. The uncertainties of other machine parameters, such as the integrated luminosity or the centre-of-mass energy, have a negligible effect on the result.

The analysis is found to be quite robust against the effects of event selection and reconstruction of the $t\bar{t}$ system. The limited acceptance and efficiency do lead to significant distortions of the distributions of $\mathcal{O}_\pm^{Re}$ and $\mathcal{O}_\pm^{Im}$. Also, the impact of migrations is clearly visible in each of the distributions. However, these effects cancel in the asymmetry. Therefore, none of these effects generate a non-zero asymmetry when the true value is 0. This type of uncertainty is referred to as *bias*. The full-simulation study shows that a spurious non-zero result due to systematic effects is expected to be smaller than 0.005.

For arbitrary values of the true asymmetry the analysis of the systematics is a bit more involved. We must also consider the possibility that the selection and reconstruction of the events lead to a non-linearity in the response to non-zero CP asymmetries $\mathcal{A}^{Re}$ and $\mathcal{A}^{Im}$. These effects are labelled as

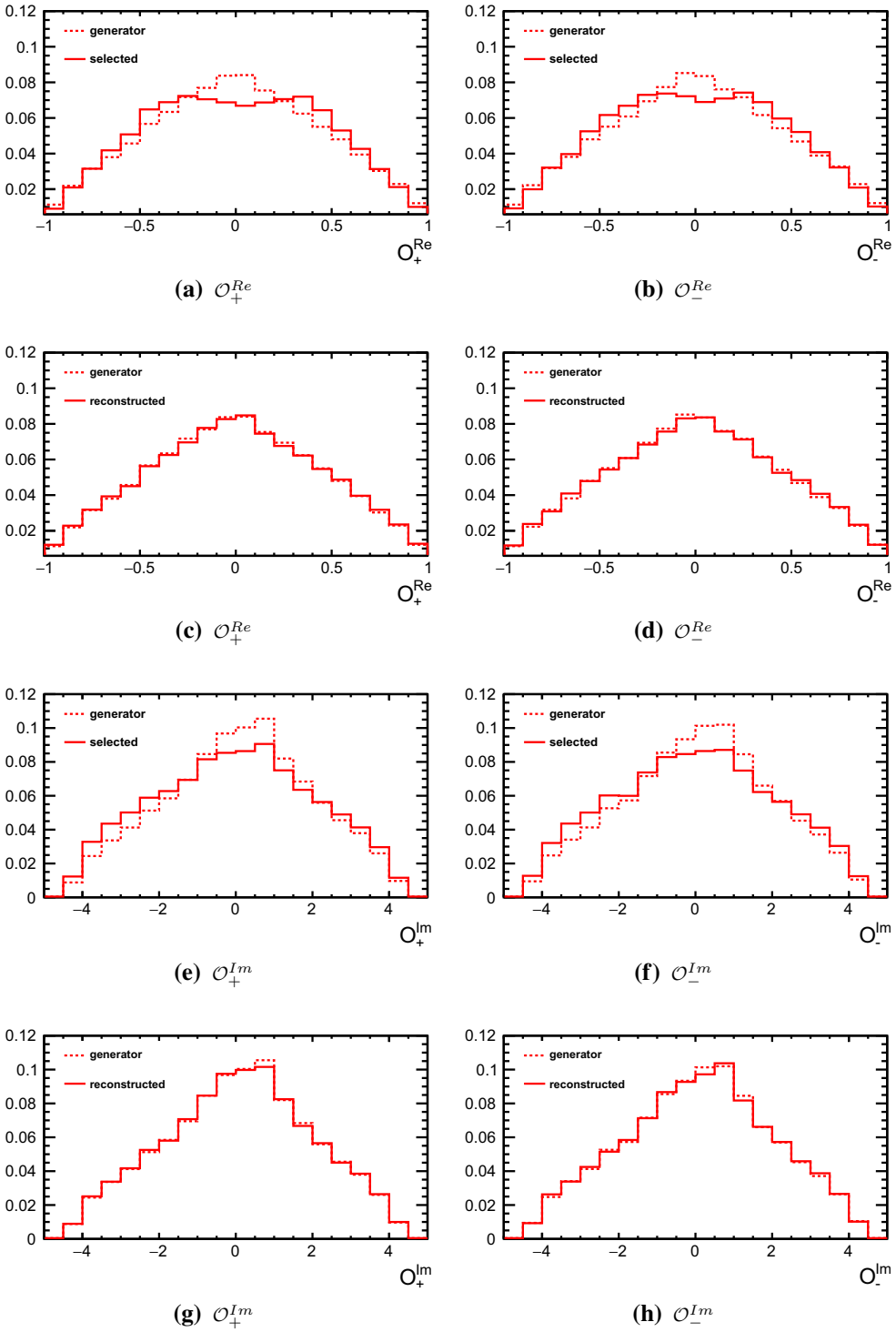

(a) $\mathcal{O}_+^{Re}$ **(b)** $\mathcal{O}_-^{Re}$

(c) $\mathcal{O}_+^{Re}$ **(d)** $\mathcal{O}_-^{Re}$

(e) $\mathcal{O}_+^{Im}$ **(f)** $\mathcal{O}_-^{Im}$

(g) $\mathcal{O}_+^{Im}$ **(h)** $\mathcal{O}_-^{Im}$

Fig. 5 The CP-odd observables $\mathcal{O}_\pm^{Re,Im}$ for CLIC at $\sqrt{s} = 3$ TeV. The two distributions correspond to the reconstructed (solid) and true (dashed) distributions for $e_L^- e_0^+$ polarization. The results for $e_R^- e_0^+$ polarization are similar. Panels **a** and **b** represent the effect of the polar angle selection on $\mathcal{O}_\pm^{Re}$. In panels **c** and **d** the impact of the angular and energy resolution on $\mathcal{O}_\pm^{Re}$ are shown. Panels **c** and **d** represent the effect of the selection on $\mathcal{O}_\pm^{Im}$, **g** and **h** the impact of the angular and energy resolution. All histograms are normalized to unit area. The $\mathcal{O}_\pm^{Im}$ distribution is truncated to the interval $[-5, 5]$

non-linearity in the following. They are evaluated in a parton-level study using events generated with non-zero WDF and EDF. Distributions and asymmetries with non-zero values of the top-quark EDF and WDF are generated using a MadGraph [71] UFO model developed in Ref. [73]. The most important cuts in the analysis, namely on the charged lepton energy, its isolation, and the polar angle of final-state quarks are applied to the six-fermion final state. The finite resolution in the reconstruction of the hadronic top-quark candidate is implemented by smearing the top-quark three-momentum vector. The migrations due to ambiguities in pairing b-jets and W-bosons at low energy are simulated by implementing the incorrect pairing for 15% of events. The selection tends to enhance the reconstructed asymmetry. This effect is particularly pronounced at very high centre-of-mass energy, where it can reach up to 10% of the true asymmetry (for $\sqrt{s} = 3$ TeV). Migrations and resolution effects dilute the asymmetry, yielding reconstructed values that are reduced by 5–15%. For centre-of-mass energies of 380 or 500 GeV migrations are the most important systematic effect. At higher energy the resolution is the dominant effect.

Theory uncertainties are estimated as follows. Radiative corrections to $t\bar{t}$ production in e^+e^- collision are known to high precision. The next-to-leading order (NLO) QCD corrections have been known for a long time [74]. The NLO electroweak corrections were determined in Refs. [75–77]. Off-shell $t\bar{t}$ production and decay including non-resonant and interference contributions at NLO QCD were investigated in Ref. [78]. The NNLO QCD corrections to $t\bar{t}$ production, including differential distributions, were calculated in [79,80]. Although not done in this work, the coefficients of $\mathrm{Re}F_{2A}^{\gamma,Z}$ and $\mathrm{Im}F_{2A}^{\gamma,Z}$ in the asymmetries of Eqs. (15) and (16) can be computed at NLO in the SM couplings. We can then estimate the theory uncertainties of these coefficients as follows. The uncertainty of the $t\bar{t}$ cross-section associated with renormalization scale variations in the range $\sqrt{s}/2 \leq \mu \leq 2\sqrt{s}$ is at NLO (NNLO) QCD about 2% (1%) at $\sqrt{s} = 380$ GeV and ~ 0.9 (0.2%) at $\sqrt{s} = 500$ GeV [80]. Assuming that the NLO SM corrections to the squared matrix element including the EDF and WDF to $t\bar{t}$ production and decay are known, we take these NLO QCD values as theory uncertainties. They are labelled "theory (non-linearity)" in Table 7. We believe that these uncertainty estimates are not unrealistic because the uncertainties of these coefficients are, in fact, associated with the expectation values $\langle \mathcal{O}_{\pm}^{Re} \rangle$, $\langle \mathcal{O}_{\pm}^{Im} \rangle$, which are ratios that are usually expanded in powers of the SM couplings. QCD scale uncertainties of expanded ratios are in general smaller than the scale uncertainty of the cross-section. An example is the top-quark forward–backward asymmetry A_{FB}^t which is known to NNLO QCD accuracy [79,80]. The scale uncertainty of the expanded A_{FB}^t is below 0.5% at these c.m. energies [80].

Table 7 The main systematic uncertainties on the asymmetry $\mathcal{A}^{Re}$ for left-handed polarized electron beam (and right-handed positron beam in the case of 500 GeV operation). Entries labelled *bias* represent estimates of upper bounds on systematic effects that yield a spurious non-zero result in the Standard Model. Entries labelled *non-linearity* represent systematic uncertainties that affect the proportionality of the response to non-zero values of the asymmetry (induced by physics beyond the Standard Model). Positive signs indicate effects that enhance the observed asymmetry. Negative signs correspond to effects that dilute the asymmetry

Source	380 GeV	500 GeV	3 TeV
Machine parameters (bias)	–	–	–
Machine parameters (non-linearity)	$<< 1\%$	$<< 1\%$	$<< 1\%$
Experimental (bias)	< 0.005	< 0.005	< 0.005
Exp. acceptance (non-linearity)	+ 3%	+ 5%	+ 10%
Exp. reconstruction (non-linearity)	− 5%	− 5%	− 15%
Theory (bias)	$<< 0.001$	$<< 0.001$	$<< 0.001$
Theory (non-linearity)	± 2%	± 0.9%	± 0.5%

The numbers in the row "theory (bias)" in Table 7 are a very conservative estimate of CP-violating SM contributions induced by higher-order W-boson exchange to $e^+e^- \to t\bar{t}$. At one loop in the electroweak couplings there are no CP-violating SM contributions to this flavour-diagonal reaction. Beyond one loop the CP-violating SM contributions to the asymmetries of Eqs. (15), (16) are smaller than $[g_W^2/(16\pi^2)]^2 \mathrm{Im}J$, where $g_W = e/\sin\theta_W$ and $\mathrm{Im}J$ is the imaginary part of a product of four quark mixing matrix elements, which is invariant under phase-changes of the quark fields. Its value is $|\mathrm{Im}J| \sim 2 \times 10^{-5}$.

The estimates of the systematic uncertainties on $\mathcal{A}^{Re}$ for several centre-of-mass energies are presented in Table 7. Our study has not found any sources of systematic uncertainty that yield a spurious asymmetry when the true asymmetry is zero. Upper limits on a systematic bias in $\mathcal{A}^{Re}$ are given in the table with the label "(bias)". Several sources can, however, enhance or dilute a non-zero true asymmetry. These are indicated as the expected relative modification of the asymmetry, with the label "(non-linearity)". Of course, these effects can be corrected to a good extent using Monte Carlo simulation. The selection bias can, moreover, be reduced by comparing the measured and predicted results in an appropriate fiducial region.

10 Prospects for CP-violating form factors

The prospects for a measurement of the top-quark form factors $F_{2A}^{\gamma,Z}$ are presented in Table 8. Rows two and three of the table show the result of our simulations described in the pre-

Table 8 The expected standard deviations (68% C.L. limits) of CP-violating form factors derived from the statistical precisions on the observables $\mathcal{O}_{\pm}^{Re,Im}$ obtained in this work. The results are compared to predictions in the literature, from fast-simulation studies in the context of the TESLA TDR [81], and from studies on the prospects at the (high-luminosity) LHC [5,82–84], on the potential of a 100 TeV proton collider [85], and of the LHeC electron–proton collider [86]

Collider	Collision	$\sqrt{s}$ (TeV)	L_{int} (ab^{-1})	Re F_{2A}^{γ}	Re F_{2A}^{Z}	Im F_{2A}^{γ}	Im F_{2A}^{Z}
Prospects derived in this study							
CLIC initial	e^+e^-	0.38	0.5	0.015	0.019	0.013	0.026
ILC initial	e^+e^-	0.5	0.5	0.005	0.007	0.006	0.010
ILC nominal	e^+e^-	0.5	4	0.002	0.003	0.002	0.004
CLIC (parton level)	e^+e^-	3	3	0.003	0.003	0.005	0.009
Previous studies for lepton colliders							
TESLA (Aguilar et al. [81])	e^+e^-	0.5	0.3	0.007	0.008	0.008	0.010
Prospects for hadron colliders							
HL-LHC (Baur et al. [82,83])	pp	14	3	0.12	0.25	0.12	0.25
HL-LHC (Röntsch and Schulze [5])	pp	14	3	–	0.16	–	–
FCChh (Mangano et al. [85])	pp	100	3	–	0.04	–	–
LHeC (Bouzas et al. [86])	ep	–	0.1	0.1	–	–	–

ceding sections for a 380 GeV stage of the Compact Linear Collider CLIC and the initial 500 GeV run at the International Linear Collider. In both cases an integrated luminosity of 500 fb^{-1} is assumed. We find that both projects have a very similar sensitivity to these form factors, reaching limits of $|F_{2A}^{\gamma}| < 0.01$ for the EDF. Assuming that systematic uncertainties can be controlled to the required level a luminosity upgrade of either of these machines may bring about a further improvement. The fourth line of Table 8 shows the prospects for the nominal ILC scenario, which envisages an integrated luminosity of 4 ab^{-1}.

The prospects for these measurements at a multi-TeV electron–positron collider are listed in the row labelled "CLIC3000" of Table 8. The sensitivity of the CP-odd observables studied in this paper to $F_{2A}^{\gamma,Z}$ increases, for $\sqrt{s} \gg 2m_t$, approximately linearly with the centre-of-mass energy. On the other hand the cross-section for $t\bar{t}$ production via s-channel Z/γ^*-boson exchange decreases as $1/s$. At linear colliders this is partly compensated by the higher luminosity at high energy: typically the instantaneous luminosity increases linearly with $\sqrt{s}$. All in all, for the 3 TeV stage of CLIC the precision is expected to be significantly higher than for the initial stage at $\sqrt{s} = 380$ GeV.

We recall here that the two-Higgs-doublet extensions of the three-generation standard model investigated in Sect. 3 give rise to sizeable form factors predominantly at centre-of-mass energies close to the $t\bar{t}$ production threshold. However, CP-violating new physics models with new heavy particles are conceivable that lead to enhancements of the CP-violating top-quark form factors $F_{2A}^{\gamma,Z}$ in the TeV energy range.

The next row in Table 8 lists the results given in the TESLA Technical Design Report [81]. The results of our full-simulation analysis are in agreement with the expectations of this parton-level study, once differences in the assumptions on polarization and integrated luminosity are taken into account.

10.1 Prospects at hadron colliders

A complete study of measurement prospects on $F_{2A}^{\gamma,Z}$ in the associated production of top-quark pairs and gauge bosons, $t\bar{t}Z$ and $t\bar{t}\gamma$, at hadron colliders was made in Refs. [82,83]. The constraints on the four CP-violating form factors are listed in Table 8 under the header "prospects for hadron colliders". These results are compared to our results for the initial ILC and CLIC stages in Fig. 6. Clearly, the measurements at hadron colliders are expected to be considerably less precise than those that can be made at lepton colliders, even after completion of the full LHC programme including the planned luminosity upgrade.

Furthermore, Table 8 summarizes the results of more recent studies of the potential of hadron colliders. The chirality-flipping terms proportional to $\sigma_{\mu\nu}$ in the effective Lagrangian used in Ref. [5] (cf. also Refs. [84,85]) differ by a factor $2m_t/m_Z \sim 4$ from our convention defined in Eq. (1). Thus the form factors F_{2A} used in this paper are related to the couplings C_{2A} of Ref. [5] by $F_{2A} = C_{2A} 2m_t/m_Z$. The 95% C.L. limits on $C_{2V/A}$ given in Refs. [5,84,85] are translated into 68% C.L. limits on $F_{2V/A}$ to facilitate comparison.

The ultimate prospects of the LHC and the luminosity upgrade depend crucially on the control of systematic uncertainties. Reference [5] finds a theory uncertainty of 15% on the total cross-section calculated at NLO precision, leading to a 20–40% improvement of the constraint on Re F_{2A}^{Z} obtained at LO. Reference [84] shows that cross-section ratios $\sigma_{t\bar{t}Z}/\sigma_{t\bar{t}}$

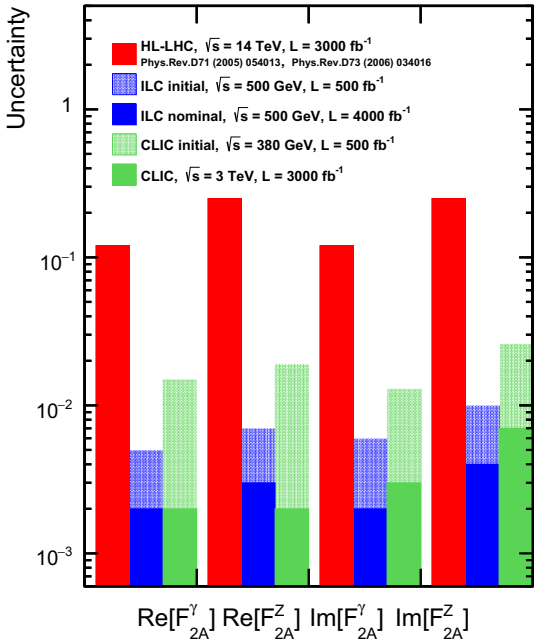

Fig. 6 Graphical comparison of 68% C.L. limits on CP-violating form factors expected at the LHC [82,83], and at the ILC and CLIC (this work). The LHC simulations assume an integrated luminosity of $\mathcal{L} = 3000\,\text{fb}^{-1}$ at 14 TeV. For the ILC we assume an initial $\mathcal{L} = 500\,\text{fb}^{-1}$ at 500 GeV and a beam polarization $P_{e^-} = \pm 0.8$, $P_{e^+} = \mp 0.3$. The nominal scenario envisages an integrated luminosity of 4 ab^{-1}. For CLIC we assume $\mathcal{L} = 500\ \text{fb}^{-1}$ at 380 GeV for the initial stage and $\mathcal{L} = 3000\ \text{ab}^{-1}$ at 3 TeV for the high-energy stage. The electron beam polarization is $P_{e^-} = \pm 0.8$ and no positron polarization is envisaged

and $\sigma_{t\bar{t}\gamma}/\sigma_{t\bar{t}}$ may be calculated to approximately 3% precision. The HL-LHC and FCChh prospects from Ref. [85] listed in Table 8 assume a systematic uncertainty of 15 and 5%, respectively.

A lepton–proton collider such as the LHeC [87] can provide constraints on anomalous top-quark electroweak couplings through measurements of the single-top production rate ($ep \to \nu t X$) and the $t\bar{t}$ photo-production rate [86]. These measurements constrain the combination of the CP-conserving and CP-violating form factors of the top-quark interaction with the photon, i.e., on F_{2V}^{γ} and F_{2A}^{γ} in the notation of Sect. 2. Assuming a large integrated luminosity (100 fb^{-1}) of energetic ep collisions ($E_p = 7$ TeV, $E_e = 140$ GeV), Ref. [86] derives the expected limit on F_{2A}^{γ} that is listed in the last row of Table 8.

10.2 Comparison to indirect constraints

Direct experimental bounds on CP-violating contributions to the $t\bar{t}Z$ and $t\bar{t}\gamma$ vertices are not available. However, with mild assumptions measurements that yield information about the Wtb vertex can be recast into limits on the form factors of the $\gamma t\bar{t}$ and $Zt\bar{t}$ interactions. In a dimension-six effective-operator framework based on the SM gauge symmetry [19,88,89] the operator O_{tW} (with Wilson coefficient C_{tW}) generates an anomalous chirality-flipping coupling g_R of the W-boson (cf. Sect. 3.3) and non-zero values for the real part of the $F_{2A}^{\gamma,Z}$ form factors in $e^+e^- \to t\bar{t}$ production. We use this approach to convert constraints from measurements of the W-helicity fractions in top-quark decay [90–92], of the single-top production cross-sections, and from studies of the polarization of W-boson in t-channel single-top production [53,93] into constraints on $F_{2A}^{\gamma,Z}$.

Reference [90] presents a combined fit to W-boson helicity fractions and single-top production cross-sections measured at the LHC, resulting in a 95% C.L. limit of $\text{Im}\,g_R \in [-0.30, 0.31]$, where g_R is one of the two chirality-flipping form factors in the $t \to Wb$ decay amplitude; see Sect. 3.3. We translate this result into a bound on $F_{2A}^{\gamma,Z}$. First we use the following expression from Ref. [19] in order to relate g_R to the Wilson coefficient C_{tW} of the effective (dimension-six) operator O_{tW}:

$$g_R = \sqrt{2} C_{tW} \frac{v^2}{\Lambda^2}. \tag{17}$$

The result of Ref. [90] can then be converted into an allowed band for Re F_{2A}^{γ} and Re F_{2A}^{Z} using the following relations[4]:

$$\text{Re}\ F_{2A}^{Z} = \sqrt{2}\left(\frac{4m_t^2}{\Lambda^2 s_W c_W}\right) \text{Im}[c_W^2 C_{tW} - s_W^2 C_{tB}] \tag{18}$$

and

$$\text{Re}\ F_{2A}^{\gamma} = \sqrt{2}\left(\frac{4m_t^2}{\Lambda^2}\right) \text{Im}[C_{tW} + C_{tB}]. \tag{19}$$

ATLAS has recently released two measurements of the decay of polarized top quarks in t-channel single-top production [53,93] and presented the 95% C.L. limit: $\text{Im}(g_R/V_L) \in [-0.18, 0.06]$. Setting $V_L = V_{tb} \sim 1$ this leads to a slightly tighter limit on the CP-violating dipole operators. The bands corresponding to both limits are drawn in Fig. 7, where the prospects listed Table 8 are also shown for comparison.

Further indirect bounds can be extracted from data at lower energies. Reference [96] used electroweak precision data to derive constraints on top-quark electroweak couplings, but CP-violating operators were not taken into account. Using in addition experimental upper bounds on the electric dipole moments of the neutron and atoms/molecules a powerful indirect constraint was derived in Refs. [97,98] on the static moment F_{2A}^{γ} of the top quark.

[4] As a cross-check the relations between form factors and Wilson coefficients in Eqs. (18) and (19) have been verified using a MadGraph [71] UFO model of the dimension-six operators that affect the top-quark electroweak vertices. The basis of the model is presented in Ref. [94]. More recent additions, in particular the extension to the CP-violating imaginary parts of the coefficients will be reported in a future publication [95]. With this setup and conversion relations we are able to reproduce several key results of Refs. [19] and [5].

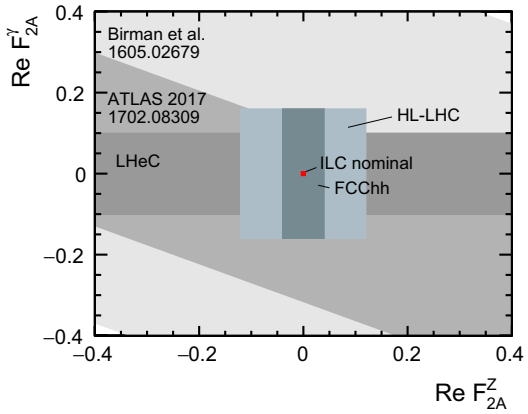

Fig. 7 The 68% C.L. limits on Re F_{2A}^{Z} and Re F_{2A}^{γ} derived from measurements of the Wtb vertex performed by ATLAS and CMS during run I of the LHC. This interpretation assumes that there is a relation between the imaginary part of the anomalous chirality-flipping coupling g_R that affects the tWb-vertex and the real part of the form factors $F_{2A}^{\gamma,Z}$ measured in $e^+e^- \to t\bar{t}$ production, as is generally the case in an effective-operator interpretation. The prospects of future colliders are indicated for comparison

11 Conclusions

CP violation in the top-quark sector is relatively unconstrained by direct measurements. While the Standard Model predicts very small effects, which are beyond the sensitivity of current and future colliders, sizeable effects may occur within well-motivated extensions of the SM. We have updated, within the type-II two-Higgs-doublet model and the MSSM, the potential magnitude of CP violation in the top-quark sector, taking into account constraints of LHC measurements. The CP-violating top-quark form factors $F_{2A}^{\gamma,Z}$ whose static limits are the electric and weak dipole moments of the top quark can be as large as 0.01 in magnitude in a viable 2HDM.

We have investigated the prospects of detecting CP violation in $t\bar{t}$ production at a future e^+e^- collider. The top spin–momentum correlations proposed in Ref. [17] for $t\bar{t}$ decay to lepton plus jets final states were evaluated with a full simulation of polarized electron and positron beams including a detailed model of the detector response. Biases due to the selection and migrations in the distributions of observables $\mathcal{O}_{\pm}^{Re}$ and $\mathcal{O}_{\pm}^{Im}$ due to ambiguities in the reconstruction of the top-quark candidates were found to cancel in the CP asymmetries $\mathcal{A}^{Re}$ and $\mathcal{A}^{Im}$ defined in Eqs. (15), (16). We expect therefore that these asymmetries, which are sensitive to the CP-violating top-quark form factors $F_{2A}^{\gamma,Z}$, are robust against such effects and can be measured with good control over experimental and theoretical systematic uncertainties. Thus, our results validate the findings of an earlier parton-level study [81] for the TESLA collider.

Measurements of these top spin–momentum correlations at a future lepton collider can provide a tight constraint on CP violation in the top-quark sector. The 68% C.L. limits on the magnitudes of the form factors $\mathrm{Re}\,F_{2A}^{\gamma,Z}$ and $\mathrm{Im}\,F_{2A}^{\gamma,Z}$ derived from our analysis of assumed 500 fb^{-1} of data collected at 380 or 500 GeV are expected to be better than 0.01. An improvement by a further factor of three may be achieved in the luminosity upgrade scenario of the ILC or in the high-energy stage of CLIC. These prospects constitute an improvement by two orders of magnitude over the existing indirect limits. With this precision, a linear collider can probe the level of CP violation in the top-quark sector predicted by a viable 2HDM model of Higgs-boson induced CP violation.

A comparison with the expectations for hadron colliders, as derived in Refs. [5,82–85], shows that the sensitivity of a future e^+e^- collider to CP-violating dipole form factors is very competitive. The constraints on form factors represent an order of magnitude improvement of the limits expected after the complete LHC programme, including the planned luminosity upgrade. The potential even exceeds that of a 100 TeV hadron collider, such as the FCChh.

Acknowledgements We would like to thank our colleagues in the ILD and CLICdp groups. The study in Sect. 6 was carried out in the framework of the ILD detector concept, that of Sect. 7 in the CLICdp collaboration. We gratefully acknowledge in particular the LCC generator group and the core software group which developed the simulation framework and produced the Monte Carlo simulation samples used in this study. We thank several members of both collaborations for a careful review of the manuscript and many helpful suggestions to improve the paper. This work benefits from services provided by the ILC Virtual Organisation, supported by the national resource providers of the EGI Federation. This research was done using resources provided by the Open Science Grid. The authors at IFIC (UVEG/CSIC) are supported under Grant MINEICO/FEDER-UE, FPA2015-65652-C4-3-R and by the "Severo Ochoa" excellence centre program, under Grant SEV-2014-0398. L. Chen is supported by a scholarship from the China Scholarship Council (CSC).

Funded by SCOAP[3].

Appendix: coefficients for $\mathcal{A}^{Re}$ and $\mathcal{A}^{Im}$

Here we give formulae for the coefficients $c_\gamma(s)$, $c_Z(s)$ and $\tilde{c}_\gamma(s)$, $\tilde{c}_Z(s)$ that determine the CP asymmetries (15) and (16), respectively. They can be represented as ratios,

$$c_\gamma(s) = \frac{N_\gamma(s)}{D(s)}, \quad c_Z(s) = \frac{N_Z(s)}{D(s)},$$
$$\tilde{c}_\gamma(s) = \frac{\widetilde{N}_\gamma(s)}{D(s)}, \quad \tilde{c}_Z(s) = \frac{\widetilde{N}_Z(s)}{D(s)}. \tag{20}$$

We compute the matrix elements for the lepton plus jets finals states at tree level, use the narrow width approximation for the intermediate t and $\bar{t}$, and integrate over the full phase space. Moreover, we neglect the width in the Z-boson propagator, since we are sufficiently far away from the Z peak and we work to lowest order in the electroweak couplings. With the conventions defined in Eqs. (1) and (3) we obtain

$$N_\gamma(s) = -\frac{4\beta_t\sqrt{s}}{3m_t}(s-m_Z^2)v_e^\gamma\Big\{(1-P_-P_+)sa_e^Z v_t^Z - (P_- - P_+)[(m_Z^2-s)v_e^\gamma v_t^\gamma - sv_e^Z v_t^Z]\Big\}, \quad (21)$$

$$N_Z(s) = -\frac{4\beta_t s^{3/2}}{3m_t}\Big\{(P_- - P_+)s(a_e^Z)^2 v_t^Z + (P_- - P_+) \times v_e^Z[(s-m_Z^2)v_e^\gamma v_t^\gamma + sv_e^Z v_t^Z] - (1-P_-P_+)a_e^Z[(m_Z^2-s)v_e^\gamma v_t^\gamma - 2sv_e^Z v_t^Z]\Big\}, \quad (22)$$

$$\widetilde{N}_\gamma(s) = \frac{2\beta_t}{15m_t^2}(16m_t^2+s)(s-m_Z^2)v_e^\gamma\Big\{(P_- - P_+)sa_e^Z v_t^Z - (1-P_-P_+)\Big[(m_Z^2-s)v_e^\gamma v_t^\gamma - sv_e^Z v_t^Z\Big]\Big\}, \quad (23)$$

$$\widetilde{N}_Z(s) = \frac{2\beta_t s(16m_t^2+s)}{15m_t^2}\Big\{(1-P_-P_+)s(a_e^Z)^2 v_t^Z + (1-P_-P_+)v_e^Z[(s-m_Z^2)v_e^\gamma v_t^\gamma + sv_e^Z v_t^Z] - (P_- - P_+)a_e^Z[(m_Z^2-s)v_e^\gamma v_t^\gamma - 2sv_e^Z v_t^Z]\Big\}, \quad (24)$$

$$D = \frac{4}{s}\Big\{(1-P_-P_+)s^2(s-4m_t^2)(v_e^Z a_t^Z)^2 + (1-P_-P_+)(s+2m_t^2)[(s-m_Z^2)v_e^\gamma v_t^\gamma + sv_e^Z v_t^Z]^2 + (1-P_-P_+)s^2(a_e^Z)^2[(a_t^Z)^2(s-4m_t^2) + (s+2m_t^2)(v_t^Z)^2] + 2(P_- - P_+)sa_e^Z\Big[v_e^Z(a_t^Z)^2 s(s-4m_t^2) + v_t^Z(s+2m_t^2)[(s-m_Z^2)v_e^\gamma v_t^\gamma + sv_e^Z v_t^Z]\Big]\Big\}, \quad (25)$$

where $P_- \equiv P_{e^-}$ and $P_+ \equiv P_{e^+}$ are the longitudinal polarization degrees of the $e^\mp$ beams, m_t and m_Z denote the mass of the t quark and Z boson, respectively, and $\beta_t = \sqrt{1-4m_t^2/s}$. The electroweak couplings of $f = e^-, t$ are

$$v_f^Z = \frac{1}{2s_W c_W}\Big(T_{3f} - 2s_W^2 Q_f\Big), \quad a_f^Z = -\frac{1}{2s_W c_W}T_{3f}, \quad v_f^\gamma = Q_f, \quad a_f^\gamma = 0, \quad (26)$$

where T_{3f} is the third component of the weak isospin of f, Q_f is the electric charge of f in units of $e > 0$, and s_W, c_W are the sine and cosine of the Weinberg mixing angle θ_W. We have neglected terms bilinear in the CP-violating form factors in the computation of the denominator D, because we know a posteriori that $|F_{2A}^{\gamma,Z}|$ must be significantly smaller than one.

References

1. M.S. Amjad et al., A precise characterisation of the top quark electro-weak vertices at the ILC. Eur. Phys. J. C **75**(10), 512 (2015). arXiv:1505.06020 [hep-ex]
2. P.H. Khiem, E. Kou, Y. Kurihara, F.L. Diberder, Probing new physics using top quark polarization in the $e^+e^- \to t\bar{t}$ process at future linear colliders. arXiv:1503.04247 [hep-ph]
3. P. Janot, Top-quark electroweak couplings at the FCC-ee. JHEP **04**, 182 (2015). arXiv:1503.01325 [hep-ph]
4. E. Devetak, A. Nomerotski, M. Peskin, Top quark anomalous couplings at the international linear collider. Phys. Rev. D **84**, 034029 (2011). arXiv:1005.1756 [hep-ex]
5. R. Röntsch, M. Schulze, Probing top-Z dipole moments at the LHC and ILC. JHEP **08**, 044 (2015). arXiv:1501.05939 [hep-ph]
6. C. Englert, M. Russell, Top quark electroweak couplings at future lepton colliders. arXiv:1704.01782 [hep-ph]
7. J. Aguilar-Saavedra, M. Fiolhais, A. Onofre, Top effective operators at the ILC. JHEP **1207**, 180 (2012). arXiv:1206.1033 [hep-ph]
8. H. Baer, T. Barklow, K. Fujii, Y. Gao, A. Hoang, S. Kanemura, J. List, H.E. Logan, A. Nomerotski, M. Perelstein, et al., The international linear collider technical design report—volume 2: physics. arXiv:1306.6352 [hep-ph]
9. T. Barklow, J. Brau, K. Fujii, J. Gao, J. List, N. Walker, K. Yokoya, ILC operating scenarios. arXiv:1506.07830 [hep-ex]
10. L. Linssen, A. Miyamoto, M. Stanitzki, H. Weerts, Physics and detectors at CLIC: CLIC conceptual design report. arXiv:1202.5940 [physics.ins-det]
11. CLICdp, CLIC Collaboration, CLIC, C. collaborations, Updated baseline for a staged compact linear collider. arXiv:1608.07537 [physics.acc-ph]
12. M.S. Amjad, M. Boronat, T. Frisson, I. Garcia, R. Poschl, E. Ros, F. Richard, J. Rouene, P.R. Femenia, M. Vos, A precise determination of top quark electro-weak couplings at the ILC operating at $\sqrt{s} = 500$ GeV. arXiv:1307.8102
13. D. Atwood, S. Bar-Shalom, G. Eilam, A. Soni, CP violation in top physics. Phys. Rept. **347**, 1–222 (2001). arXiv:hep-ph/0006032
14. G.L. Kane, G.A. Ladinsky, C.P. Yuan, Using the top quark for testing standard model polarization and CP predictions. Phys. Rev. D **45**, 124–141 (1992)
15. D. Atwood, A. Soni, Analysis for magnetic moment and electric dipole moment form-factors of the top quark via $e^+e^- \to t\bar{t}$. Phys. Rev. D **45**, 2405–2413 (1992)
16. W. Bernreuther, O. Nachtmann, P. Overmann, T. Schroder, Angular correlations and distributions for searches of CP violation in top quark production and decay. Nucl. Phys. B **388**, 53–80 (1992). [Erratum: Nucl. Phys.B 406, 516 (1993)]
17. W. Bernreuther, P. Overmann, Probing Higgs boson and supersymmetry induced CP violation in top quark production by (un)polarized electron–positron collisions. Z. Phys. C **72**, 461–467 (1996). arXiv:hep-ph/9511256 [hep-ph]
18. A. Juste et al., Report of the 2005 Snowmass top/QCD working group, ECONFC0508141:PLEN0043 (2005). arXiv:hep-ph/0601112
19. J.A. Aguilar-Saavedra, A minimal set of top anomalous couplings. Nucl. Phys. B **812**, 181–204 (2009). arXiv:0811.3842 [hep-ph]
20. W. Bernreuther, P. Galler, C. Mellein, Z.G. Si, P. Uwer, Production of heavy Higgs bosons and decay into top quarks at the LHC. Phys. Rev. D **93**(3), 034032 (2016). arXiv:1511.05584 [hep-ph]

21. G.C. Branco, P.M. Ferreira, L. Lavoura, M.N. Rebelo, M. Sher, J.P. Silva, Theory and phenomenology of two-Higgs-doublet models. Phys. Rep. **516**, 1–102 (2012). arXiv:1106.0034 [hep-ph]
22. W. Bernreuther, T. Schroder, T.N. Pham, CP violating dipole form-factors in $e^+e^- \to t\bar{t}$. Phys. Lett. B **279**, 389–396 (1992)
23. CMS Collaboration, Precise determination of the mass of the Higgs boson and tests of compatibility of its couplings with the standard model predictions using proton collisions at 7 and 8 TeV. Eur. Phys. J. C **75**(5), 212 (2015). arXiv:1412.8662 [hep-ex]
24. ATLAS Collaboration, Measurements of the Higgs boson production and decay rates and coupling strengths using pp collision data at $\sqrt{s} = 7$ and 8 TeV in the ATLAS experiment. Eur. Phys. J. C **76**(1), 6 (2016). arXiv:1507.04548 [hep-ex]
25. ATLAS, CMS Collaboration, Measurements of the Higgs boson production and decay rates and constraints on its couplings from a combined ATLAS and CMS analysis of the LHC pp collision data at $\sqrt{s} = 7$ and 8 TeV. JHEP **08**, 045 (2016). arXiv:1606.02266 [hep-ex]
26. CMS Collaboration, Study of the mass and spin-parity of the Higgs boson candidate via its decays to Z boson pairs. Phys. Rev. Lett. **110**, 081803 (2013). arXiv:1212.6639 [hep-ex]
27. ATLAS Collaboration Collaboration, Evidence for the spin-0 nature of the Higgs boson using ATLAS data. Phys. Lett. B **726**, 120–144 (2013). arXiv:1307.1432 [hep-ex]
28. S. Berge, W. Bernreuther, J. Ziethe, Determining the CP parity of Higgs bosons at the LHC in their tau decay channels. Phys. Rev. Lett. **100**, 171605 (2008). arXiv:0801.2297 [hep-ph]
29. ATLAS Collaboration, Measurements of the properties of the Higgs-like boson in the four lepton decay channel with the ATLAS detector using 25 fb^{-}1 of proton–proton collision data. ATLAS-CONF-2013-013 (2013)
30. CMS Collaboration, Search for a pseudoscalar boson decaying into a Z boson and the 125 GeV Higgs boson in $\ell^+\ell^- b\bar{b}$ final states. Phys. Lett. B **748**, 221–243 (2015). arXiv:1504.04710 [hep-ex]
31. ATLAS Collaboration, Search For Higgs boson pair production in the $\gamma\gamma b\bar{b}$ final state using pp collision data at $\sqrt{s} = 8$ TeV from the ATLAS detector. Phys. Rev. Lett. **114**(8), 081802 (2015). arXiv:1406.5053 [hep-ex]
32. ATLAS Collaboration, Search for a CP-odd Higgs boson decaying to Zh in pp collisions at $\sqrt{s} = 8$ TeV with the ATLAS detector. Phys. Lett. B **744**, 163–183 (2015). arXiv:1502.04478 [hep-ex]
33. CMS Collaboration, Search for a Higgs boson in the mass range from 145 to 1000 GeV decaying to a pair of W or Z bosons. JHEP **10**, 144 (2015). arXiv:1504.00936 [hep-ex]
34. ATLAS, CMS Collaboration, Y. Nagai, Higgs search in $b\bar{b}$ signatures at ATLAS and CMS. PoS Beauty **2013**, 001 (2013). arXiv:1306.1784 [hep-ex]
35. CMS Collaboration, Search for resonant pair production of Higgs bosons decaying to two bottom quark–antiquark pairs in proton–proton collisions at 8 TeV. Phys. Lett. B **749**, 560–582 (2015). arXiv:1503.04114 [hep-ex]
36. CMS Collaboration, Search for neutral MSSM Higgs bosons decaying to a pair of tau leptons in pp collisions. JHEP **10**, 160 (2014). arXiv:1408.3316 [hep-ex]
37. ATLAS Collaboration, Search for neutral Higgs bosons of the minimal supersymmetric standard model in pp collisions at $\sqrt{s} = 8$ TeV with the ATLAS detector. JHEP **11**, 056 (2014). arXiv:1409.6064 [hep-ex]
38. ATLAS Collaboration, TA Collaboration, Search for heavy Higgs bosons A/H decaying to a top-quark pair in pp collisions at $\sqrt{s} = 8$ TeV with the ATLAS detector
39. T. Hermann, M. Misiak, M. Steinhauser, $\bar{B} \to X_s\gamma$ in the two Higgs doublet model up to next-to-next-to-leading order in QCD. JHEP **11**, 036 (2012). arXiv:1208.2788 [hep-ph]
40. A. Kobakhidze, N. Liu, L. Wu, J. Yue, Implications of CP-violating top-Higgs couplings at LHC and Higgs factories. Phys. Rev. D **95**(1), 015016 (2017). arXiv:1610.06676 [hep-ph]
41. M. Pospelov, A. Ritz, Electric dipole moments as probes of new physics. Ann. Phys. **318**, 119–169 (2005). arXiv:hep-ph/0504231 [hep-ph]
42. A. Bartl, E. Christova, T. Gajdosik, W. Majerotto, Electroweak dipole moment form-factors of the top quark in supersymmetry. Nucl. Phys. B **507**, 35–50 (1997). arXiv:hep-ph/9705245 [hep-ph]. [Erratum: Nucl. Phys. B 531, 653 (1998)]
43. W. Hollik, J.I. Illana, S. Rigolin, C. Schappacher, D. Stockinger, Top dipole form-factors and loop induced CP violation in supersymmetry. Nucl. Phys. B **551**, 3–40 (1999). arXiv:hep-ph/9812298 [hep-ph]. [Erratum: Nucl. Phys. B 557, 407 (1999)]
44. A. Arbey, J. Ellis, R.M. Godbole, F. Mahmoudi, Exploring CP violation in the MSSM. Eur. Phys. J. C **75**(2), 85 (2015). arXiv:1410.4824 [hep-ph]
45. E. Christova, M. Fabbrichesi, Supersymmetric CP violations and T odd observables in $t\bar{t}$ and W^+W^- physics. Phys. Lett. B **315**, 338–348 (1993). arXiv:hep-ph/9302315 [hep-ph]
46. W. Bernreuther, P. Overmann, CP asymmetries in top quark pair production and decay: contributions from neutral Higgs boson and gluino exchange. Z. Phys. C **61**, 599–606 (1994)
47. B. Grzadkowski, CP violation in t anti-t production at e^+e^- colliders. Phys. Lett. B **305**, 384–391 (1993). arXiv:hep-ph/9303204 [hep-ph]
48. A. Bartl, E. Christova, W. Majerotto, CP violating asymmetries in top quark production and decay in e^+e^- annihilation within the MSSM. Nucl. Phys. B **460**, 235–251 (1996). arXiv:hep-ph/9507445 [hep-ph]. [Erratum: Nucl. Phys. B 465, 365 (1996)]
49. W. Hollik, J.I. Illana, C. Schappacher, D. Stockinger, S. Rigolin, Dipole form-factors and loop induced CP violation in supersymmetry. arXiv:hep-ph/9808408
50. W. Adam, Searches for SUSY. Proceedings, 38th International Conference on High Energy Physics (ICHEP 2016)PoS(ICHEP2016)017. https://pos.sissa.it/282/017/
51. ATLAS Collaboration, Search for direct production of charginos and neutralinos in events with three leptons and missing transverse momentum in $\sqrt{s} = 8$TeV pp collisions with the ATLAS detector. JHEP **04**, 169 (2014). arXiv:1402.7029 [hep-ex]
52. CMS Collaboration, Measurement of the W boson helicity in events with a single reconstructed top quark in pp collisions at $\sqrt{s} = 8$ TeV. JHEP **01**, 053 (2015). arXiv:1410.1154 [hep-ex]
53. ATLAS Collaboration, Search for anomalous couplings in the Wtb vertex from the measurement of double differential angular decay rates of single top quarks produced in the t-channel with the ATLAS detector. JHEP **04**, 023 (2016). arXiv:1510.03764 [hep-ex]
54. W. Bernreuther, P. Gonzalez, M. Wiebusch, The top quark decay vertex in standard model extensions. Eur. Phys. J. C **60**, 197–211 (2009). arXiv:0812.1643 [hep-ph]
55. S.D. Rindani, Effect of anomalous t b W vertex on decay lepton distributions in $e^+e^- \to t\bar{t}$ and CP violating asymmetries. Pramana **54**, 791–812 (2000). arXiv:hep-ph/0002006
56. B. Grzadkowski, Z. Hioki, Decoupling of anomalous top decay vertices in angular distribution of secondary particles. Phys. Lett. B **557**, 55–59 (2003). arXiv:hep-ph/0208079
57. W. Kilian, T. Ohl, J. Reuter, WHIZARD: simulating multi-particle processes at LHC and ILC. Eur. Phys. J. C **21**, 1742 (2011). arXiv:0708.4233 [hep-ph]
58. H. Abramowicz et al., The international linear collider technical design report—volume 4: detectors. arXiv:1306.6329 [physics.ins-det]
59. W. Kilian, T. Ohl, J. Reuter, WHIZARD: simulating multi-particle processes at LHC and ILC. Eur. Phys. J. C **71**, 1742 (2011). arXiv:0708.4233 [hep-ph]

60. J. Fuster, I. García, P. Gomis, M. Perelló, E. Ros, M. Vos, Study of single top production at high energy electron positron colliders. Eur. Phys. J. C **75**, 223 (2015). arXiv:1411.2355 [hep-ex]
61. T. Sjostrand, S. Mrenna, P.Z. Skands, PYTHIA 6.4 physics and manual. JHEP **05**, 026 (2006). arXiv: hep-ph/0603175
62. GEANT4 Collaboration, S. Agostinelli et al., GEANT4: a simulation toolkit. Nucl. Instrum. Methods A **506**, 250–303 (2003)
63. J. Marshall, M. Thomson, The Pandora software development kit for particle flow calorimetry. J. Phys. Conf. Ser. **396**, 022034 (2012)
64. M. Boronat, J. Fuster, I. Garcia, E. Ros, M. Vos, A robust jet reconstruction algorithm for high-energy lepton colliders. Phys. Lett. B **750**, 95–99 (2015). arXiv:1404.4294 [hep-ex]
65. LCFI Collaboration, D. Bailey et al., The LCFIVertex package: vertexing, flavour tagging and vertex charge reconstruction with an ILC vertex detector. Nucl. Instrum. Methods A **610**, 573–589 (2009). arXiv:0908.3019 [physics.ins-det]
66. T. Suehara, T. Tanabe, LCFIPlus: a framework for jet analysis in linear collider studies. Nucl. Instrum. Methods A **808**, 109–116 (2016). arXiv:1506.08371 [physics.ins-det]
67. P. Doublet, F. Richard, R. Poschl, T. Frisson, J. Rouene, Determination of top-quark asymmetries at the ILC. arXiv:1202.6659 [hep-ex]
68. J.S. Marshall, A. Münnich, M.A. Thomson, Performance of particle flow calorimetry at CLIC. Nucl. Instrum. Methods A **700**, 153–162 (2013). arXiv:1209.4039 [physics.ins-det]
69. A. Abdesselam et al., Boosted objects: a probe of beyond the standard model physics. Eur. Phys. J. C **71**, 1661 (2011). arXiv:1012.5412 [hep-ph]
70. M. Boronat, J. Fuster, I. Garcia, P. Roloff, R. Simoniello, M. Vos, Jet reconstruction at high-energy lepton colliders. arXiv:1607.05039 [hep-ex]
71. J. Alwall, R. Frederix, S. Frixione, V. Hirschi, F. Maltoni, O. Mattelaer, H.S. Shao, T. Stelzer, P. Torrielli, M. Zaro, The automated computation of tree-level and next-to-leading order differential cross sections, and their matching to parton shower simulations. JHEP **07**, 079 (2014). arXiv:1405.0301 [hep-ph]
72. M. Beckmann, J. List, A. Vauth, B. Vormwald, Spin transport and polarimetry in the beam delivery system of the international linear collider. JINST **9**, P07003 (2014). arXiv:1405.2156 [physics.acc-ph]
73. S.K. Gupta, A.S. Mete, G. Valencia, CP violating anomalous top-quark couplings at the LHC. Phys. Rev. D **80**, 034013 (2009). arXiv:0905.1074 [hep-ph]
74. J. Jersak, E. Laermann, P.M. Zerwas, Electroweak production of heavy quarks in e^+e^- annihilation. Phys. Rev. D **25**, 1218 (1982). [Erratum: Phys. Rev. D 36, 310 (1987)]
75. W. Beenakker, S.C. van der Marck, W. Hollik, e^+e^- annihilation into heavy fermion pairs at high-energy colliders. Nucl. Phys. B **365**, 24–78 (1991)
76. J. Fleischer, A. Leike, T. Riemann, A. Werthenbach, Electroweak one loop corrections for e^+e^- annihilation into $t\bar{t}$ including hard bremsstrahlung. Eur. Phys. J. C **31**, 37–56 (2003). arXiv:hep-ph/0302259
77. T. Hahn, W. Hollik, A. Lorca, T. Riemann, A. Werthenbach, $O(\alpha)$ electroweak corrections to the processes $e^+e^- \to \tau^-\tau^+, c\bar{c}, b\bar{b}, t\bar{t}$: A Comparison, in Extended joint ECFA/DESY study on physics and detector for a linear e+ e- collider. Proceedings, Summer Colloquium, Amsterdam, Netherlands, April 4, 2003. arXiv:hep-ph/0307132. http://alice.cern.ch/format/showfull?sysnb=2382496
78. B. Chokoufé Nejad, W. Kilian, J.M. Lindert, S. Pozzorini, J. Reuter, C. Weiss, NLO QCD predictions for off-shell $t\bar{t}$ and $t\bar{t}H$ production and decay at a linear collider. JHEP **12**, 075 (2016). arXiv:1609.03390 [hep-ph]
79. J. Gao, H.X. Zhu, Top quark forward–backward asymmetry in e^+e^- annihilation at next-to-next-to-leading order in QCD. Phys. Rev. Lett. **113**(26), 262001 (2014). arXiv:1410.3165 [hep-ph]
80. L. Chen, O. Dekkers, D. Heisler, W. Bernreuther, Z.-G. Si, Top-quark pair production at next-to-next-to-leading order QCD in electron positron collisions. JHEP **12**, 098 (2016). arXiv:1610.07897 [hep-ph]
81. ECFA/DESY LC Physics Working Group Collaboration, J.A. Aguilar-Saavedra et al., TESLA: the superconducting electron positron linear collider with an integrated x-ray laser laboratory. Technical design report. Part 3. Physics at an e^+e^- linear collider. arXiv:hep-ph/0106315
82. U. Baur, A. Juste, L.H. Orr, D. Rainwater, Probing electroweak top quark couplings at hadron colliders. Phys. Rev. D **71**, 054013 (2005). arXiv:hep-ph/0412021
83. U. Baur, A. Juste, D. Rainwater, L.H. Orr, Improved measurement of ttZ couplings at the CERN LHC. Phys. Rev. D **73**, 034016 (2006). arXiv:hep-ph/0512262
84. M. Schulze, Y. Soreq, Pinning down electroweak dipole operators of the top quark. Eur. Phys. J. C **76**(8), 466 (2016). arXiv:1603.08911 [hep-ph]
85. M.L. Mangano et al., Physics at a 100 TeV pp collider: standard model processes. arXiv:1607.01831 [hep-ph]
86. A.O. Bouzas, F. Larios, Probing ttγ and ttZ couplings at the LHeC. Phys. Rev. D **88**(9), 094007 (2013). arXiv:1308.5634 [hep-ph]
87. LHeC Study Group Collaboration, J.L. Abelleira Fernandez et al., A large hadron electron collider at CERN: report on the physics and design concepts for machine and detector. J. Phys. G **39**, 075001 (2012). arXiv:1206.2913 [physics.acc-ph]
88. B. Grzadkowski, M. Iskrzynski, M. Misiak, J. Rosiek, Dimension-six terms in the standard model Lagrangian. JHEP **10**, 085 (2010). arXiv:1008.4884 [hep-ph]
89. C. Zhang, S. Willenbrock, Effective-field-theory approach to top-quark production and decay. Phys. Rev. D **83**, 034006 (2011). arXiv:1008.3869 [hep-ph]
90. J.L. Birman, F. Déliot, M.C.N. Fiolhais, A. Onofre, C.M. Pease, New limits on anomalous contributions to the Wtb vertex. Phys. Rev. D **93**(11), 113021 (2016). arXiv:1605.02679 [hep-ph]
91. CMS Collaboration, Measurement of the W-boson helicity in top-quark decays from $t\bar{t}$ production in lepton+jets events in pp collisions at $\sqrt{s} = 7$ TeV. JHEP **10**, 167 (2013). arXiv:1308.3879 [hep-ex]
92. ATLAS Collaboration, Measurement of the W boson polarization in top quark decays with the ATLAS detector, JHEP **06**, 088 (2012). arXiv:1205.2484 [hep-ex]
93. ATLAS Collaboration, Probing the W tb vertex structure in t-channel single-top-quark production and decay in pp collisions at $\sqrt{s} = 8$ TeV with the ATLAS detector. JHEP **04**, 124 (2017). arXiv:1702.08309 [hep-ex]
94. O. Bessidskaia Bylund, F. Maltoni, I. Tsinikos, E. Vryonidou, C. Zhang, Probing top quark neutral couplings in the standard model effective field theory at NLO in QCD. JHEP **05**, 052 (2016). arXiv:1601.08193 [hep-ph]
95. G. Durieux, M. Perello, M. Vos, C. Zhang, Global constraints on top effective field theory at lepton colliders (in preparation)
96. J. de Blas, M. Chala, J. Santiago, Renormalization group constraints on new top interactions from electroweak precision data. JHEP **09**, 189 (2015). arXiv:1507.00757 [hep-ph]
97. V. Cirigliano, W. Dekens, J. de Vries, E. Mereghetti, Is there room for CP violation in the top-Higgs sector? Phys. Rev. D **94**(1), 016002 (2016). arXiv:1603.03049 [hep-ph]
98. V. Cirigliano, W. Dekens, J. de Vries, E. Mereghetti, Constraining the top-Higgs sector of the standard model effective field theory. Phys. Rev. D **94**(3), 034031 (2016). arXiv:1605.04311 [hep-ph]